UNIVERSITY OF OKLAHOMA

GRADUATE COLLEGE

ANALYSIS OF ILLUMINATION INTENSITY IN FOURIER PTYCHOGRAPHY MICROSCOPY

A THESIS

SUBMITTED TO THE GRADUATE FACULTY

in partial fulfillment of the requirements for the

Degree of

MASTER OF SCIENCE

By JOSEPH LUCAS

Norman, Oklahoma

2025

ANALYSIS OF ILLUMINATION INTENSITY IN

FOURIER PTYCHOGRAPHY MICROSCOPY

A THESIS APPROVED FOR THE

SCHOOL OF ELECTRICAL AND COMPUTER ENGINEERING

BY THE COMMITTEE CONSISTING OF

Dr. Yuchen Qiu, Chair

Dr. Joseph Havlicek

Dr. Javier Jo Pun Kay

TABLE OF CONTENTS

ABSTRACT

Fourier Ptychography Microscopy (FPM) is a computational imaging technique that achieves high-resolution, wide-field microscopy by combining multiple low-resolution images captured under varying illumination angles. While the method has demonstrated resolution beyond the traditional diffraction limit, its practical application remains constrained by long image acquisition times. This research investigates the limiting factors of the current 32×32 LED illumination array and explores modifications to improve illumination performance and reduce exposure time. Using optical power measurements, oscilloscope analysis, and controlled imaging trials, the study identifies multiplexing frequency and short duty cycles to be the primary factors affecting LED brightness resulting in longer capture times. Comparative experiments with custom-designed 5×5 and 7×7 matrices driven by static DC signals show a significant increase in optical power output and smoother illumination uniformity, leading to short exposure times. The findings highlight the impact of illumination stability on Fourier domain sampling and provide practical guidelines for developing LED arrays optimized for high-speed, high-fidelity FPM imaging.

CHAPTER 1

1.1 INTRODUCTION

High-resolution imaging is fundamental to advances in biomedical research, materials science, and engineering, yet traditional microscopy techniques remain limited by physical constraints such as the diffraction limit. Computational imaging approaches, including Fourier Ptychography Microscopy (FPM), have emerged as powerful methods to overcome these barriers by synthesizing high-resolution images from multiple low-resolution acquisitions taken under varied illumination angles. FPM offers significant advantages in terms of resolution, field of view, and cost-effectiveness, making it an attractive tool for both research and applied settings. Each image requires exposure time for enough light to enter the aperture to produce an image bright enough to process. The total exposure time increases with each image taken, which compounds with the increase in the grid size used. This thesis aims to reduce the exposure time of each image by enhancing the illumination methods used in current versions of FPM image acquisition methods. This chapter will cover a brief history of FPM's origins and current research, then discuss the specific goals, methodology, significance and limitations.

1.2 BACKGROUND

Fourier Ptychography Microscopy (FPM) is a computational imaging technique that reconstructs a high-resolution image by combining multiple low-resolution images captured under varied illumination angles. In conventional microscopy, there exists a fundamental tradeoff between resolution and field of view (FoV). Traditional imaging systems are constrained by the space-bandwidth product (SBP), a concept that describes the maximum amount of information an optical system can acquire. Higher resolution typically comes at the expense of smaller FoV, and vice versa. This limitation is dictated by the physical parameters of the optical system, particularly the numerical aperture (NA) of the objective lens and the pixel size of the image sensor. To image small features, one must increase magnification, which improves resolution by enlarging the projected features on the detector. However, increased magnification simultaneously narrows the observable area. This tradeoff becomes particularly problematic in applications such as digital pathology or cell culture monitoring, where scientists must assess both large-scale structures and single-cell features. FPM was developed to overcome this fundamental limitation.

Since its initial demonstration [1], FPM has developed a wide range of improvements aimed at both reconstruction quality and acquisition speed. Illumination strategies such as multiplexed patterns and grid reshaping have been proposed to optimize angular coverage and sampling efficiency. On the computational side, advances in phase retrieval algorithms and, more recently, deep learning approaches have accelerated image reconstruction while improving robustness to noise and system aberrations.

Some researchers have discovered optimal methods of multiplexing—using multiple illumination angles per image—to reduce the number of images taken [2, 3]. Crucially, the limitations in acquiring several (sometimes hundreds) images compound on each other, increasing the time requirement for a single reconstruction. Any reduction in the time required in a single image capture will pay off multiplicatively to however many images are needed for any method of reconstruction.

1.3 RESEARCH PROBLEM

From FPM's inception, the Adafruit 32×32 LED array used has been an easy to acquire hardware option and has been used as a benchmark for further research. While FPM leverages many angles of illumination to detect slight changes in the Fourier domain to create a super resolution image, it suffers from the large time cost associated with taking a picture at each angle that correlates to the number of LEDs used in the illumination array. Simply increasing the magnification with the objective lens can be expensive and will still incur the tradeoff of FoV, however FPM will maintain a wide FoV with greater magnification with far less cost. The appeal of the FPM process is that it works on any level of magnification suitable for optical microscopy. There are impressive benefits to multiplexing and array shapes that can have significant impact on the quantity of images taken when multiple angles can be combined. What seems to be missing from the research, however, is data and experimentation focusing on reducing the image capture time per image. Regardless of the illumination strategy or computational method used to create the reconstruction image, if each image capture time can be reduced, that will snowball into a much larger effect as number of images increases.

1.4 RESEARCH AIM, OBJECTIVES, QUESTIONS

The primary goal of this research is to identify and characterize the limiting factors of the current 32×32 LED array used in the FPM platform, and to determine how these limitations can be mitigated or redesigned to enable faster image acquisition without sacrificing reconstruction quality. Because the total imaging duration of FPM is directly constrained by the exposure time required for each LED illumination, this work focuses on understanding and adjusting the parameters that most strongly influence exposure time.

Specifically, this involves measuring the optical power output at the source as well as distances practical for FPM imaging. It also involves testing the array geometry variables, such as inter-LED spacing and distance between the array and sample plane. Additionally, different LED types will be used and tested to compare output potential at various heights. Each test will look at raw picture analytics, as well as image reconstruction to ensure proper comparisons are being made.

This study aims to investigate the limitations of the widely used Adafruit 32×32 LED array used in the FPM platform and explore potential modifications to enhance imaging efficiency. To guide this investigation, the following research questions are proposed:

1. What variables can affect the brightness of an image?
2. How will exposure time be affected by changes in those variables?

1.5 RESEARCH SIGNIFICANCE

This research contributes to the advancement of Fourier Ptychography Microscopy by isolating the role of LED brightness in reducing exposure time during image acquisition. While the study identifies many bottlenecks, the findings demonstrate that illumination hardware remains a critical variable influencing overall efficiency. By systematically examining LED intensity within the constraints of a low-cost, reproducible setup, the work provides a clearer understanding of how illumination design can be optimized in resource-limited environments.

At the research level, these results inform future efforts to design FPM systems that balance affordability with performance, offering practical insights into how component selection affects data collection rates. More broadly, improvements in FPM efficiency have the potential to accelerate biological and medical imaging workflows, enabling faster, higher-throughput analysis of microscopic samples. By highlighting the potential and limitations of illumination-driven strategies, this research lays groundwork for innovations that could expand the availability and impact of computational microscopy in science and healthcare research.

1.6 LIMITATIONS

One major limitation to FPM lies in the time required to collect sample images. Although the goal is to minimize the total acquisition time over an image set, there are several system components that introduce delays, including the camera, the computer, and the method of file saving. In practice, the camera proved to be the dominant source of delay. Once the microscope was calibrated, the camera could capture full-resolution images (5472 x 3648 pixels) at a rate of roughly 1 frame per second or, in some cases, as low as 0.4 frames per second. The cause of the slow nature of image capturing is unknown and could be a boon to further explore upgrades for this project.

The research conducted aims to test LED intensity as a factor of exposure time in the FPM system. While other methods of illumination like hemispherical illumination and multiplexed illumination affect the illumination angle or combinations of angles, this study focuses on the role of LED brightness. Likewise, laser lights are not utilized in this data sample collection. Restrictions to basic off-the-shelf components were adhered to which keeps the production of such systems low cost and simpler to replicate. Any computational algorithms beyond that of the traditional one image per LED is beyond the scope of this research. While many factors contribute to the effectiveness of the FPM system, the scope remained confined to LED spacing and brightness control in order to create concise results without too many contributing variables.

Limitations were also imposed in the creation of custom PCBs designed for the newer grids. Each custom PCB was created using a desktop milling machine with limitations in accuracy, and minimum trace widths. The milling machine is a subtractive process—only able to cut away at the top and bottom copper layers, so no protective layers, solder masks, or vias were added through the machining process. Without advanced machining processes, the PCBs were designed to be assembled by hand and were not miniaturized to densely pack in LEDs for the sake of being error prone during assembly.

The ability to increase the brightness and thus reduce exposure time during image data collection is the primary goal of this research. While there is a benefit to adjusting the illumination source and other peripheral devices, another one of the key limiting factors turned out to be the camera used for the experiment. Full-resolution images were 38.1 MB in size and were displayed on screen with around 0.4 to 1 frame per second. Without synchronizing the frame rate with the LED switching time, the minimum time to guarantee the new image is $\frac{2}{FPS}$ when factoring potential aliasing. At 0.4 FPS, the time delay for a new image could be up to 5 seconds. This issue is further convolved with the image capture time which can take up to 2 seconds. This vastly overshadows much of our realizable gains due to the limitations in the image capture phase. Without the intervention of a management program run on the PC controlling the image capture software, Mosaic, the total time of the imaging phase would include human timing errors and were therefore removed from the quantitative data.

For the purposes of testing the efficacy of the LED hardware, the calculations will focus on exposure time which will isolate the illumination hardware, rather than the camera hardware and human operation that imposes the largest bottlenecks for this experiment. While the results provide insight into how LED brightness impacts exposure time in an FPM system, the broader applicability of these findings is constrained by the hardware configuration. Because the study relies on low-cost, commercially available components, the conclusions are most relevant to similar low-resource or replicable FPM setups. Systems employing advanced cameras, faster data transfer protocols, or alternative illumination strategies may experience different limiting factors and performance outcomes.

1.7 STRUCTURAL OUTLINE

Chapter 1 introduces Fourier Ptychography Microscopy (FPM), outlining its origins, theoretical foundations, and its role in addressing the fundamental tradeoff between resolution and field of view. The motivation for this study is presented, along with the objectives and scope, including the limitations that shape the research focus.

Chapter 2 presents a review of relevant literature, examining both theoretical and practical developments in FPM. Key areas of prior work are discussed, including illumination strategies such as multiplexed and hemispherical arrays, computational advances, and hardware considerations influencing system performance. This review identifies gaps in the current research, which provides the basis for investigating LED brightness as a factor in acquisition efficiency.

Chapter 3 describes the methodology used in this study. The experimental design is outlined in detail, including the optical configuration, LED arrays, and camera system employed.

Calibration procedures, data collection protocols, and analytical methods are explained, with particular emphasis on how LED intensity was varied and measured in relation to image acquisition performance.

Chapter 4 presents the results of the experiments. Findings are reported with respect to power output, exposure time, and the influence of LED brightness and type on sample acquisition. Where appropriate, results are supported with figures, quantitative comparisons, and analysis to demonstrate the relationship between illumination conditions and system performance.

Chapter 5 provides more in-depth discussion of these findings in the context of existing literature and theoretical expectations. The implications of increasing LED brightness are considered along with array geometry, as are the practical limitations imposed by hardware constraints. This chapter provides a quantified and illustrative context to the reduction of exposure time achieved.

Finally, Chapter 6 offers concluding remarks. The major contributions of the study are summarized, highlighting the role of LED intensity in reducing exposure time while acknowledging the bottlenecks introduced by other hardware and software. The broader impact of the work is discussed. The thesis concludes with recommendations for future research, including opportunities for hardware and software upgrades.

CHAPTER 2: LITERATURE REVIEW

2.1 CONVENTIONAL MICROSCOPY LIMITATIONS

Optical microscopy has been a central tool for the biological and physical sciences, providing the ability to observe structures and processes otherwise invisible to the naked eye. However, traditional optical systems are fundamentally constrained by the relationship between resolution and field of view (FoV). This tradeoff is formalized through the concept of the space-bandwidth product (SBP), which defines the maximum information capacity of an imaging system. The SBP depends on both the numerical aperture (NA) of the objective lens (how much light a lens can collect) and the physical pixel size of the image sensor.

Higher resolution can be achieved by increasing magnification, which enlarges fine features on the detector and improves the ability to resolve small details. The limits of resolution are dictated by the NA of the objective lens and the wavelength of light, as described by Abbe's diffraction limit (1). Similarly, the FoV is constrained by the pixel size and sensor area of the camera used for image capture.

$$d = \frac{\lambda}{2NA} \tag{1}$$

While the experiments described in this thesis do not make attempts to use FPM to circumvent the diffraction limit, FPM as computational microscopy has the ability to do so with the proper setup [4].

2.2 FPM PRINCIPALS AND ORIGINS

The original publication on FPM [1] brought to the scientific community a way of iteratively stitching together variably illuminated, low-resolution images to produce a high-resolution wide-field image. By leveraging the power of optical microscopy and computational algorithms, they were able to produce a large SBP.

At its core, FPM is a computational imaging technique that achieves high-resolution, wide FOV (super-resolution) images by combining multiple low-resolution intensity images captured under different illumination angles. The algorithm reconstructs a high-resolution complex sample field in Fourier space.

Based around a simple microscope with the illumination source below the sample, the microscope objective with a limited NA captures a low-resolution patch of the Fourier domain spectrum in each image. With each additional angle of illumination behind the sample, the resultant image shifts slightly in the Fourier domain, revealing more frequency information. The algorithm iteratively stitches together the information in the Fourier domain space and is reconstructed into its real components in the final image reconstruction. Reconstruction produces a higher resolution image without sacrificing the field of view that is present in the original image.

2.3 ILLUMINATION STRATEGIES IN FPM

To make the best of an optical system, it is imperative that the lens captures as much light from the specimen as possible. The NA of the system, based on (Eq. 2), posits n as the index of refraction, and μ as the half-angle of the cone of light the lens can accept.

$$NA = n \cdot sin(\mu) \quad (2)$$

A full view lens with a 90-degree half-angle would equate to a hemisphere and would yield sin(90) to be 1 under perfect conditions. With the other variable being the medium, open air has a refractive index of 1 and could be replaced with a more favorable medium such as an immersion oil [5].

$$f_{LED} = \frac{1}{\lambda}\frac{D_{LED}}{\sqrt{(D_{LED})^2 + h^2}} \quad (3)$$

$$R_{LED} = \frac{f_{obj}}{f_{LED}} = NA\frac{\sqrt{(D_{LED})^2 + h^2}}{D_{LED}} \quad (4)$$

$$\mathrm{R_{overlap}} = \begin{cases} \frac{1}{\pi}\left[2arccos\left(\frac{1}{2R_{LED}}\right) - \frac{1}{R_{LED}}\sqrt{1-\left(\frac{1}{2R_{LED}}\right)^2}\right], & x < 0 \\ 0, & else \end{cases} \quad (5)$$

Equations 3-5 set up the framework for understanding the frequency coverage in the FPM image [6]. Ultimately these equations culminate to (Eq. 5) where we determine the overlap of the LEDs based on their spacing between each other and their height. $R_{overlap}$ is a measure of the percentage of an LEDs illumination area on the sensor that is also covered by another LEDs illumination area. The two methods of increasing $R_{overlap}$ is to increase the distance of the array to the sample, or to reduce the spacing between the individual LEDs. In that paper, the authors recommend $R_{overlap}$ to be larger than 31.81% to guarantee FPM without pixel aliasing issues. This research is fundamental to getting adequate reconstruction detail and will be crucial to the experimentation done in this thesis studying the illumination intensity.

Other methods of illumination involve multiplexing to reduce the quantity of individual images taken per grid. Tian, et al. correctly identified the slow capturing phase that is inhibited by long exposure times and is spread out over hundreds of LEDs in many cases [2]. The authors circumvent this time-consuming phase by flashing on four to eight LEDs simultaneously to reduce the image capture phase drastically. They recognize an $R_{overlap} > 60\%$ is required in multiplexing for sufficient coverage of the Fourier space, and their experimental results are comparable to the single LED method. They report to be able to effectively reduce the image capture phase of 293 images from 586 seconds to 74 seconds without sacrificing image quality [2].

In another multiplexing experiment, Lin et al. were able to find the impact of each LED and reduced the total LEDs to only ones with the most significant impact on the overall reconstruction. In addition, multiple methods of multiplexing ensued with the reduced LED count leading to a total of 56 images from a 225 LED grid [3]. In doing so, the experiment not only reinforces multiplexing as an adequate image capture reduction method but also identifies high-impact LED placement on a rectangular grid.

2.4 COMPUTATIONAL ADVANCES IN FPM

Of the advances in computation, one of the main contributions relies in the reduction of data to be processed, such as in multiplexing. Since the images are not only high-resolution images, but also there can be hundreds of images per image set, the computation time increases rapidly. Using image processing techniques in the spatial and spectral domain, the effect of redundancy across an image found that when eliminated, can reduce the multi-exposure and impact the acquisition time by about 50% [7]. Additionally, the rise in convolutional neural networks has found a use case in FPM by aiding in the image processing [8]. Combining this technique with FPM by training on an initial dataset of images, researchers were able to more rapidly reconstruct a new set of live culture images in a dynamic environment [9].

2.5 HARDWARE CONSIDERATIONS

The hardware used in the FPM setup is simple, only requiring a camera, tube lens, objective lens and the LED array. The technical limitation is only in the alignment of the stages and can be assembled using many of the products sold by Thor Labs [10]. Notably, attaining measurements at the micrometer scale will require precise alignment and is recommended to have lab equipment that can provide that level of fidelity. Much of the equipment is not technically complicated and the LED arrays can vary from off-the-shelf models [1] to custom built arrays [5, 10].

2.6 GAPS IN THE LITERATURE

Much of the literature seeks to remove the additional time costs associated with FPM through computational methods like multiplexing [2, 5], and spacing the LEDs out far enough to achieve a similar reconstruction without sacrificing much in the way of quality [7]. The primary avenue of improvement I seek to address in this research is the effect of LED brightness and how the variables associated with its intensity can be manipulated in favor of image quality or a reduction in image capture time.

CHAPTER 3: METHODOLOGY

3.1 SYSTEM SETUP

This experiment employs a traditional FPM configuration composed of an illumination module, a sample stage, an optical imaging system, and a camera. At the base of the system is a height-adjustable stand that supports a rectangular LED matrix and an Arduino UNO R3 with a compatible ‘shield’ that interfaces the microcontroller to the LED matrix used to control the illumination sequence. Figure 1 illustrates the microscope system diagram where the LED array (A) provides programmable angled illumination to the sample slide (B), which is mounted at various heights above the grid. Light transmitted through the sample then passes sequentially through a NIKON 4x/0.13 numerical aperture objective lens (C), a tube lens (D), and finally reaches the camera sensor (E) positioned at the top of the optical stack.

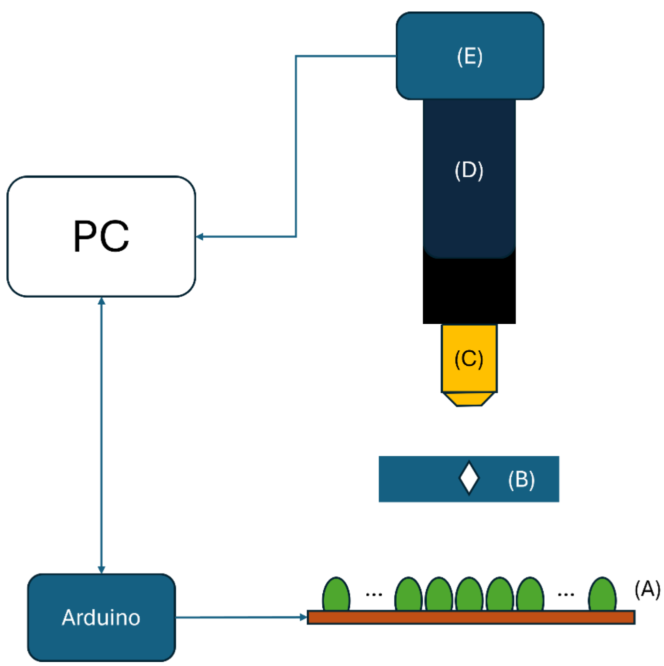

Figure 1: FPM System Diagram

The camera is calibrated to focus on approximately infinity so that the image sensor records the angular (Fourier domain) information of the sample rather than its direct spatial image. This allows the light that passes through the objective lens to travel approximately parallel through the tube lens to the camera sensor instead of converging or diverging. Optically, focusing on infinity places the image sensor in the far field of the sample, where the recorded intensity corresponds to the spatial frequency components required for Fourier reconstruction. This configuration allows each illumination angle from the LED array to sample a shifted region of the sample's Fourier spectrum, which is central to the FPM computation model.

The infinity calibration was achieved by focusing the camera on a distant object outside the laboratory—specifically, a stadium light post at the OU Tennis Club approximately 2,700 feet away from the Stephenson Research Center (Appendix: Figure 34). Based on a 70-millimeter spacing between the LED grid and the sample, the ratio of 2,700 feet to 70 millimeters yields approximately 11,756, a value sufficiently large to approximate infinity focus for this setup. This alignment ensures that the optical system captures necessary far-field diffraction information for accurate Fourier domain reconstruction.

The sample used in this experiment is Newport's HIGHRES-2 Super High Resolution Air Force Test Target, which conforms to the 1951 U.S. Air Force MIL-STD-150A specification. Per the manufacturer's datasheet, the target has a minimum feature size of 137 nanometers (Table 2), well below the diffraction limit of the 4x/0.13 objective lens, making it an ideal specimen for evaluating the super-resolution capability of the FPM reconstruction process.

Figure 2: Newport HIGHRES-2 Test Target

Spatial Frequency (cycles per millimeter)								
Element Number	**Group Number**							
	4	**5**	**6**	**7**	**8**	**9**	**10**	**11**
1	16.0	32.0	64.0	128.0	256.0	512.0	1,024	2,048
2	18.0	35.9	71.8	143.7	287.4	574.7	1,149	2,299
3	20.2	40.3	80.6	161.3	322.5	645.1	1,290	2,580
4	22.6	45.3	90.5	181.0	362.0	724.1	1,448	2,896
5	25.4	50.8	101.6	203.2	406.4	812.7	1,625	3,251
6	28.5	57.0	114.0	228.1	456.1	912.3	1,825	3,649

Table 1: Spatial Frequency of Newport HIGHRES-2 Test Target

Bar/Space Width Calculations (microns)	
Element Number	**Group Number**

	4	**5**	**6**	**7**	**8**	**9**	**10**	**11**
1	31.250	15.625	7.813	3.906	1.953	0.977	0.488	0.244
2	27.841	13.920	6.960	3.480	1.740	0.870	0.435	0.218
3	24.803	12.402	6.201	3.100	1.550	0.775	0.388	0.194
4	22.097	11.049	5.524	2.762	1.381	0.691	0.345	0.173
5	19.686	9.843	4.922	2.461	1.230	0.615	0.308	0.154
6	17.538	8.769	4.385	2.192	1.096	0.548	0.274	0.137

Table 2: Bar/Space Width of Newport HIGHRES-2 Test Target

3.2 LED POWER OUTPUT

Measuring the optical power output of the original 32×32 off-the-shelf LED matrix was an essential step in establishing a baseline for system performance. Since the array contains 1,024 individual LEDs—significantly more than the number implemented in the prototype versions—the brightness sampling was limited to the central 7×7 region to enable a practical and representative comparison. Power measurements of all LED arrays were collected following a consistent order, beginning at the central LED and proceeding outward in a counterclockwise spiral pattern, concluding at the bottom-right corner of the selected grid (Figure 3).

Figure 3: Image Collection Order

The off-the-shelf 32×32 LED array employs integrated LED controllers to manage the large number of emitters through a multiplexing technique, which rapidly switches LEDs on and off at a frequency imperceptible to the human eye. However, this switching behavior was suspected to reduce the overall effective brightness, thereby necessitating longer exposure times during image acquisition. To mitigate this limitation, the custom LED matrices developed for this experiment were designed to operate using a direct current (DC) signal. Operating under DC conditions is expected to provide a higher constant illumination intensity and consequently allow for reduced exposure times and improved image brightness. Additionally, the resistors used in the custom matrices were carefully selected to maximize the safe allowable current for the LEDs and the Arduino output pins, ensuring optimal brightness while maintaining safe operating conditions for the control hardware.

Using a Thorlabs PM400 Optical Power Meter, the brightness will be measured by placing the sensor at the same distance from the LED array as the sample stage was during the image capture. Each LED matrix will be measured to their central 49 LEDs, except for the 5×5 matrix that only has 25 in total. One further brightness measurement will take place at the LED source to provide a maximum output that can be used for reference.

With the switch to direct current established, we will reduce the overall component count that will reduce the circuit complexity as thus prevent assembly errors as well as reduce costs. However, there are still challenges associated with the physical parameters of the LEDs, the Arduino shields, and the circuit milling process that must be considered during the design phase.

3.3 CUSTOM PCB DESIGN

The initial experiments utilized a 32×32 off-the-shelf LED grid, composed of surface-mount (SMD) RGB LEDs and supported by open-source Arduino software. The array interfaces with the Arduino UNO R3 microcontroller through a dedicated shield (also an off-the-shelf purchasable component) that connects to the board's I/O pins and routes control signals via a 16-pin ribbon cable. The grid also requires separate power and ground connections and, depending on configuration, allows daisy-chaining to additional panels. However, for traditional FPM applications—where only one LED is illuminated at a time—much of this expansion capability and additional power handling was unnecessary. The primary focus instead became understanding and improving individual LED brightness and exposure behavior to determine which characteristics could be optimized in future designs.

Because the original 32×32 array contains 1,024 LEDs, significantly more than needed for a proof-of-concept system, a smaller 5×5 prototype was developed as the first redesign. This reduction of grid size accelerated prototyping while still providing meaningful insight into illumination control and image reconstruction quality. The replacement LEDs were standard 5-millimeter through-hole components, chosen for their availability and ease of use in early testing. However, their larger physical size required an increased inter-LED spacing of 7 millimeter, compared to the 4 millimeter spacing in the commercial array. Increasing the size of the LED, and in turn, the LED spacing effects the $R_{overlap}$ (5) for a fixed array height. Consequently, altering the effective angular resolution achievable by the system assuming no other changes are made. However, with the assumption that the illumination output will be increased, the through-hole LEDs should be able to perform at a comparable level when placed further from the sample as to maintain a similar $R_{overlap}$.

The 5×5 matrix was designed to be integrated directly into the Arduino's shield, eliminating the need for a separate LED board or a secondary connection such as a ribbon cable (Appendix: Figure 35-35). In this configuration, the Arduino UNO R3 outfitted with the 5×5 LED matrix shield was mounted directly beneath the sample, forming a compact, single-unit illumination module. However, this design introduced several fabrication and spatial challenges. The fixed I/O pin spacing on the Arduino, for example, limited the available routing area, and the large footprint of the 5-millimeter LEDs further constrained layout options (Appendix: Figure 36). To minimize costs, the prototype PCBs were fabricated in-house using a circuit milling machine. This practice prevents using very small trace widths that would be typical of a modern circuit board (around 8 mils) and requires a safer width (35 mils) to prevent destroying the thinner traces that are hard to manufacture. Additionally, the absence of a solder mask increased the likelihood of short circuits during manual soldering, especially when working near exposed ground planes. These factors required a larger overall footprint and more generous clearances to avoid thermal damage that could lead to component failure during assembly.

One of the practical challenges that confronted the successful assembly of the 5×5 grid was that the shape of the LED bulb prevented ensuring a solid connection at the top layer of the copper. Without access to vias, soldering the LEDs to the shield was restricted to the bottom side only. This itself added another layer of complexity, as both the anodes and cathodes were only accessible from the bottom layer as a result. When routing traces for a rectangular matrix like this, it is typical to route in horizontal and vertical traces. For example, when a row of anodes are given a high signal and a column of cathodes are given a low signal, only the intersection of the row and column will pass current. Practically speaking, weaving horizontal and vertical traces on the bottom copper layer was not possible given the constraints of a small board with comparatively large traces. To fix this issue, one additional drill point was marked per LED as a point where one pin could be routed up to the orthogonal trace, allowing the circuit logic to be used (Figure 4). As a replacement for vias, the clipped LED legs were soldered into the additional holes and connected the trace to the top and bottom layers.

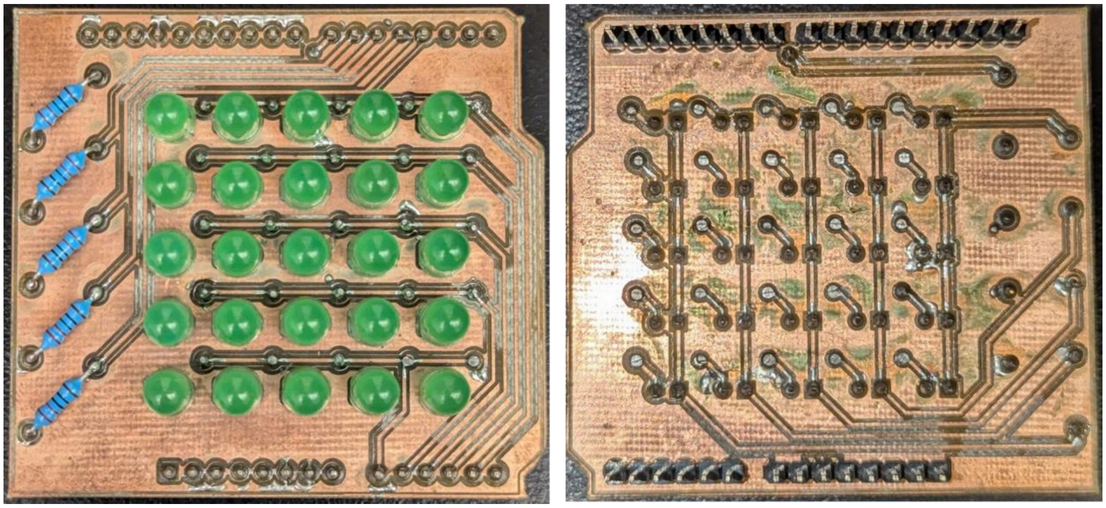

Figure 4: 5×5 PCB (LEFT) Top (RIGHT) Bottom

Building on the 5×5 experience, a 7×7 matrix redesign was implemented to both improve brightness and better match the geometry of the original 32×32 array. 0608 surface-mount LEDs were selected to provide higher illumination intensity in a smaller package. The reduced component size restored the 4-millimeter spacing of the previous commercial grid, thereby removing spacing as a variable and enabling more direct comparisons of illumination uniformity and overlap between systems. As with the 5×5 design, routing the anode and cathode traces in a single PCB layer remained challenging. Without the sturdy scraps of the through hole LEDs to fill in for the lack of vias, solid-core wire was used as jumpers to bridge traces that switched layers. While effective, this approach was time-intensive and occasionally compromised connection integrity. Heat conduction was a concern since the components on the 7×7 grid are small enough to need constant contact on the pads in order to stay in place. While the copper and solder heated up enough for solder to flow the via joint, the heat would be transferred to the other side and reflow the LED out of place or create an unreliable joint.

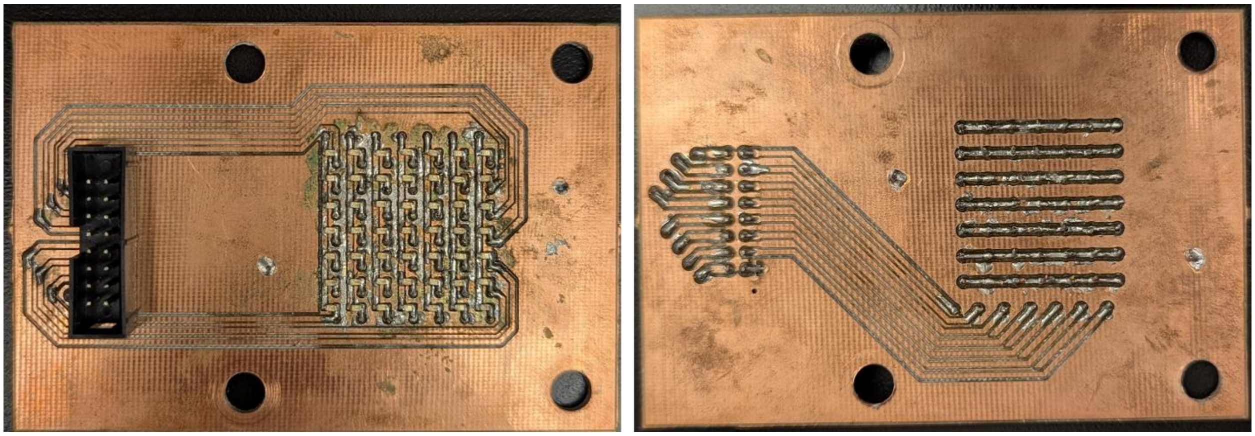

Figure 5: 7×7 PCB (LEFT) Top (RIGHT) Bottom

All circuit boards were designed using KiCAD, a free and open-source PCB design suite (Appendix: Figure 35-38). The custom LED matrices were configured to operate on a direct-current (DC) signal, unlike the multiplexed commercial grid that employed fast on-off switching via integrated LED controllers. The multiplexing approach, while sufficient for display applications, can reduce effective brightness and increase required exposure times during image capture. Operating the custom boards on a DC signal provides a constant illumination intensity, leading to shorter exposure times and brighter images overall. To support this configuration, current-limiting resistors were selected to maximize brightness while maintaining safe operating limits for the Arduino output pins, ensuring reliable and stable performance across all experiments.

3.4 IMAGE ACQUISITION

After installing each tested LED array and calibrating the microscope, an initial image was taken. For each set of images, parameters are noted during the image capture phase to gather data on LED matrix distance from sample, LED spacing, and exposure time per image. These data points provide a basis for evaluating performance and identifying potential improvements when compared with the control (32×32) grid. Once the initial parameters are logged, the images are collected in the image capture order (Figure 3) using lossless compression such as TIFF or PNG formats.

For the current FPM system, a specialized software governs the image capture phase, taking one picture after another automatically through the imaging software, then sending a signal to the Arduino to illuminate the next LED in the sequence, and repeating until the sequence completed. While this would help greatly in the automation process in the future, the custom arrays used keyboard input through the serial interface terminal emulator PuTTY to communicate basic functions to the Arduino: on/off toggle, up, down, left, right, and center. The inability for this version of the Arduino code to interact with the imaging software removes the potential for quantifying the total time comparison between each LED matrix.

3.5 BRIGHTNESS CHARACTERIZATION METHOD

Brightness in the image samples are controlled primarily by the exposure time during capture. The bright field is the area on the LED array that the objective lens has direct 'line of sight' of. These create bright images that have high contrast and are the center-most LEDs. The dark field images are taken by LEDs outside that interior area, but still interact with the sample, and their diffraction patterns still provide information to the Fourier space. Figure 6 illustrates the bright field inside the red circle and the dark field outside the red circle extending out to increasing darkness.

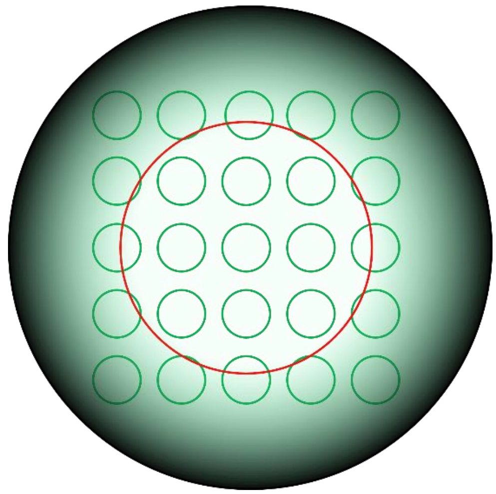

Figure 6: Illustration of bright field and dark field

Ideally, the image sets gathered will be comprised of both a bright field subset and the dark field subset, so care is taken to not initially overexpose the bright field to compensate for the low visibility of the dark field. If a brightfield image is exposed too high, the amplitude of the light around the edges of the features on the sample have the potential to peak at the highest brightness value, which is a 16-bit value in this case. This has potential for data loss, as the comparative brightness can no longer be measured beyond the maximum value. This tends to happen around the hard edges of objects on the sample, including dust artifacts such as in Figure 7.

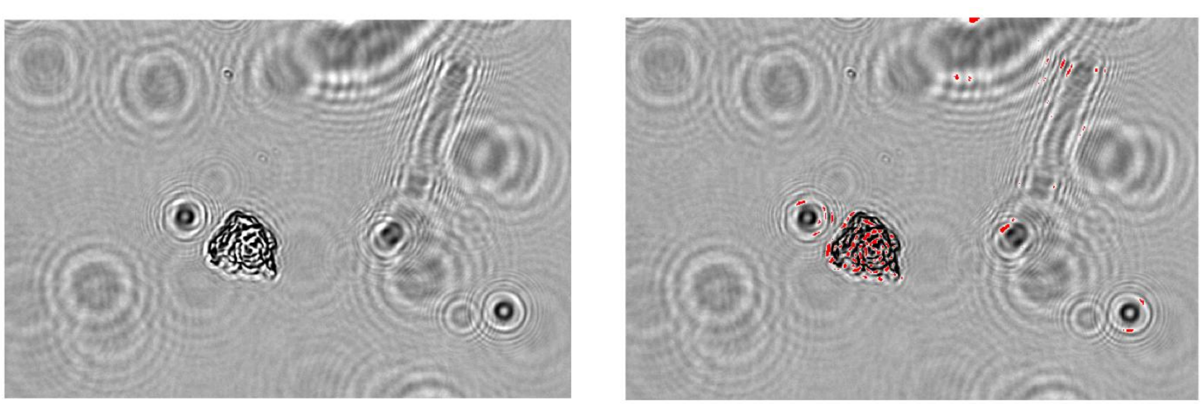

Figure 7: (Left) Peaking brightness in raw image. (Right) Peaking brightness highlighted in red.

For accurate comparisons, histograms will be generated to ensure similar ranges of values in brightness as well as an attempt to reduce the number of peak-value pixels. The primary objective in this stage is to attempt very similar histogram profiles through Mosaic's histogram viewer, so that the exposure times to be referenced against each other are known to have a similar overall brightness, so that there is a reliable common ground for comparison when changing the LED type, grid spacing, and grid height.

3.6 FINAL PROCESSING AND EVALUATION APPROACH

After the entire 25 or 49 image set is completed, the images are processed by the FPM program in MATLAB. By including the data set, the LED geometry in relation to the sample, as well as the optical parameters the program produces the reconstructed image. The resulting images after FPM reconstruction show amplitude and phase as well as the pupil function calculations. Ideally, the improvements made to the hardware will have noticeable impact on the final image reconstruction, but again, the goal to reduce time capturing images through exposure time.

The evaluation of a successful experiment will rely on the exposure time saved and comparative quality in both the raw and reconstructed images. Since the microscope equipment used in this setup does not approach the smallest feature size on the USAF sample, even after reconstruction, the smallest discernable features will appear to fuse together or disappear entirely. The smallest feature size will be measured with a brightness graph of a vertical cross-section running through the horizontal lines. Knowing that there are three horizontal lines per element in a group, the cross-sectional analysis should show a commensurate peak and valley of pixel brightness for each horizontal line. If the cross section does not indicate all three lines in the graph, then the feature size is not discernable.

Since the brightness and quality of the LEDs are different for each array, their grading will be based on their exposure times, histogram content, and distance from the sample plane. For each of those scenarios, each grid will be compared to the others with one unchanged variable to see the performance of the other grids under the same conditions—in both raw input and final reconstructions. For example, keeping the distance from the sample plane and same exposure time will vary in histogram content. If those conditions can be met, the data should reveal a potential best-case scenario to extrapolate from and provide the best practices in designing FPM LED arrays.

CHAPTER 4: EXPERIMENTAL RESULTS

4.1 LED POWER OUTPUT

Each grid's LED power output is measured by using a Thorlabs PM400 Optical Power Meter at the 532-nanometer wavelength (green light). With the sensor placed directly on top of the illuminated LED, the central 7×7 region of the 32×32 matrix emitted a mean optical power of 64.24 microwatts per LED. In comparison, the custom 5×5 matrix using 5-millimeter bulb LEDs produced 1.9 milliwatts, while the 7×7 array composed of 0608 surface-mount LEDs yield an even higher mean output of 3.1 milliwatts **(**Figure 8**)**. This demonstrates roughly an order of magnitude increase in optical power between the off-the-shelf 32×32 grid and the custom matrices. Such a dramatic difference in LED intensity implies that the required exposure settings during image acquisition will vary drastically.

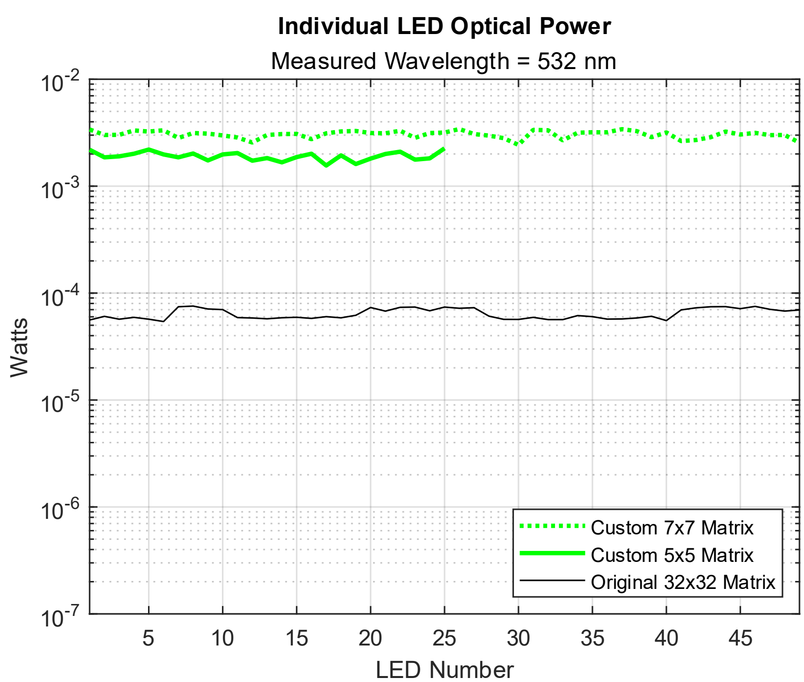

Figure 8: Individual LED optical power output at the source collected in illumination sequence

Oscilloscope measurements revealed that the 32×32 matrix's LED controller integrated circuits operate the LEDs using pulse-width modulation (PWM) at 167 hertz (6 millisecond period) with a 5% duty cycle (0.3 millisecond active on time). This design is practical for its intended hobbyist applications. It minimizes power consumption and prevents visible flickers to the human eye. The multiplexing technique also allows the Arduino UNO R3 microcontroller to control all 1024 LEDs with a limited number of output pins. However, under the FPM imaging setup, this pulsing introduces a synchronization challenge.

The camera's exposure time must be aligned with the LED refresh rate, otherwise the resulting image exhibits periodic brightness artifacts. Figure 9 clearly shows a horizontal banding pattern caused by desynchronization between the LED pulses and the camera exposure. When an LED is pulsed, its brightness ramps up and down as current transitions through the dielectric material. At higher frequencies, a greater proportion of each cycle is spent in these transition states, reducing the effective optical power output. For clarity, the specific RGB LEDs used in the 32×32 grid are not likely to be the direct cause of the reduction in brightness, rather their 5% active duty cycle is likely the largest contributor of the low performance.

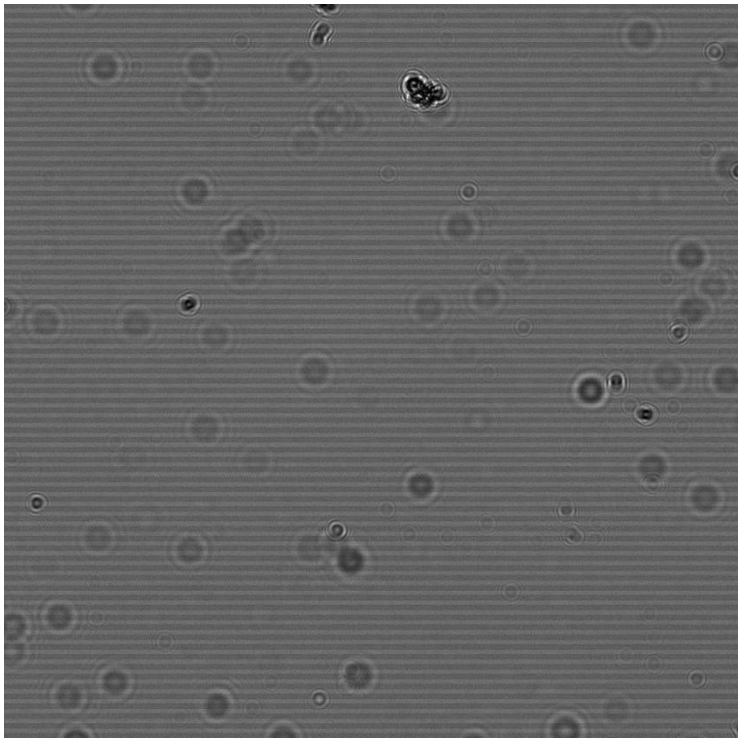

Figure 9: Effect of desynchronized camera exposure and 32×32 matrix frequency

The multiplexed driving scheme of the 32×32 grid also introduces a ghosting artifact. The board refreshes its four 16x16 quadrants sequentially, and each quadrant appears to weakly activate the same column the LED in the row directly below the active one. This leeching current slightly illuminates unintended LEDs at lower intensity termed 'ghosting' (Figure 10). When the active LED is in the bottom row of a quadrant, the ghosting activity occurs not in the top row of the quadrant beneath it, but on the top row of the same quadrant. While the precise impact on the FPM reconstruction is unclear, this is likely a hardware-level issue that can be corrected in future LED array revisions.

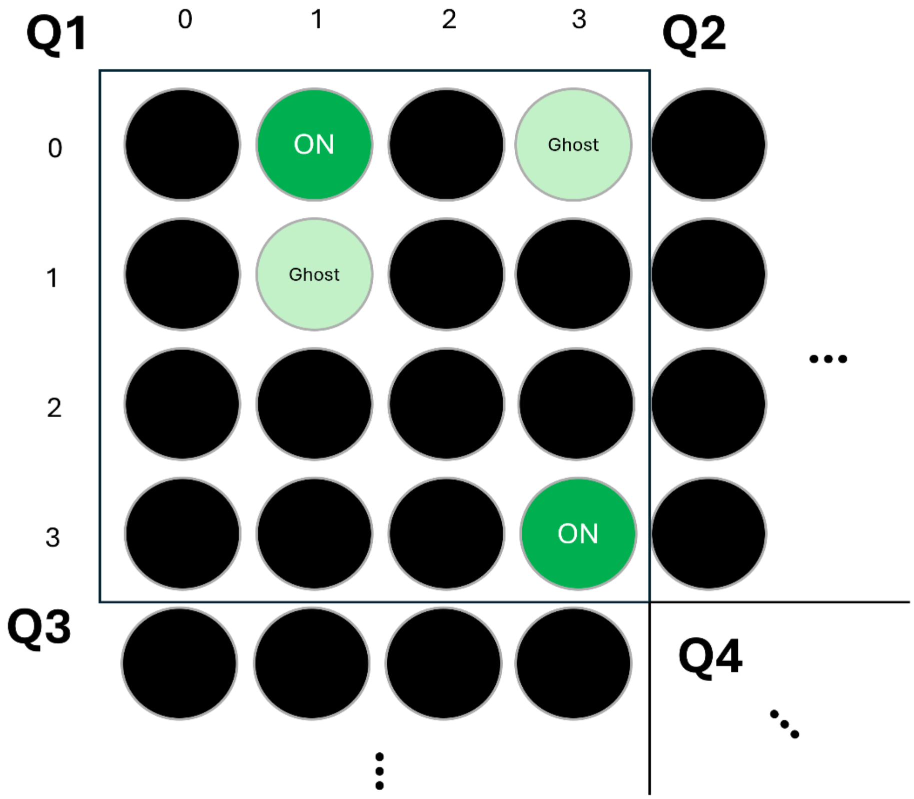

Figure 10: Simplified illustration of ghosting effect on 32×32 grid

While Figure 8 illustrates the direct power output of each LED used in each grid as close to the source as possible, that data does not show what the sample stage will receive. Getting power values that reach the sample stage are a much better indicator for the impact of the final image and can be directly seen by the raw images. Understanding that with each new array geometry and brightness change caused by the LED or the signaling microcontroller (PWM versus DC power), each grid is placed at a variety of heights while the optical power sensor is placed at the sample stage. The heights vary depending on the grid, as the array geometry dictates to some degree the most ideal range for a grid size and brightness. For reference, for standard operation of the 32×32 grid in the lab at the research facility, the distance is typically around 70-72 millimeters.

Because the 32×32 grid's low per-LED output requires significant gain to produce visible images, an additional measurement was performed to evaluate the power received at the sample plane across different LED heights. Figure 11 shows the expected inverse-square falloff in illumination intensity as distance increases, along with an additional decrease for LEDs positioned further from the optical axis in the spiral acquisition sequence. The effect can be seen exagerated with image sequences that were taken closer to the sample plane, while the effect proves to level out further away, indicating that there is a tradeoff of brightness at the sample plane with a relatively balanced brightness per LED further away. This analysis confirms that illumination geometry and distance both play a critical role in the effective exposure and reconstruction quality.

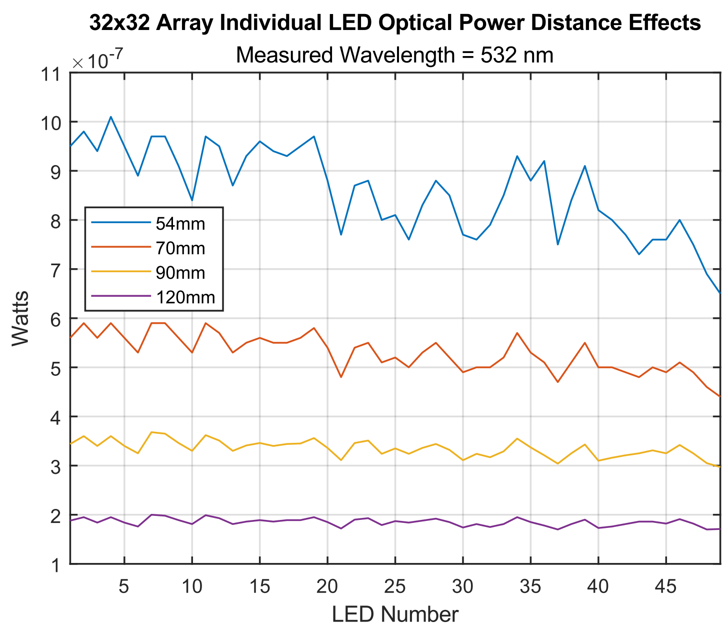

Figure 11: 32×32 grid optical power received by sample at various distances

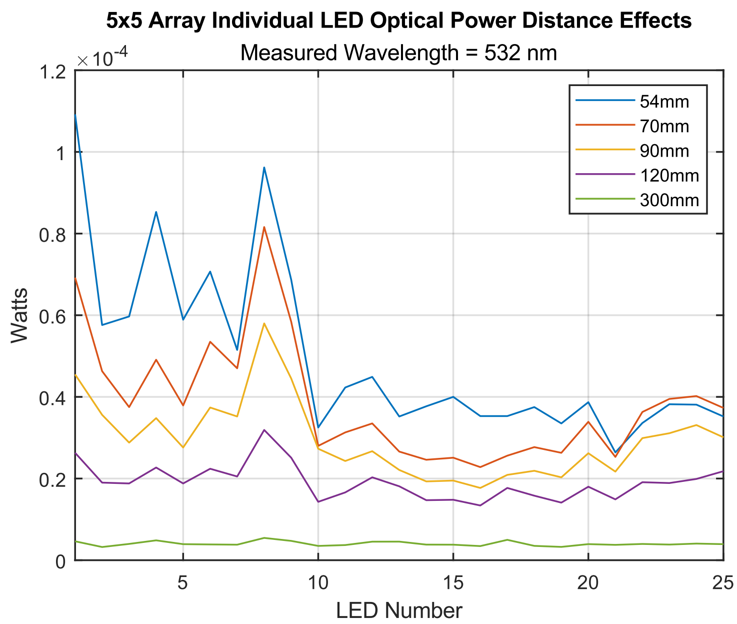

Figure 12: 5×5 grid optical power received by sample at various distances

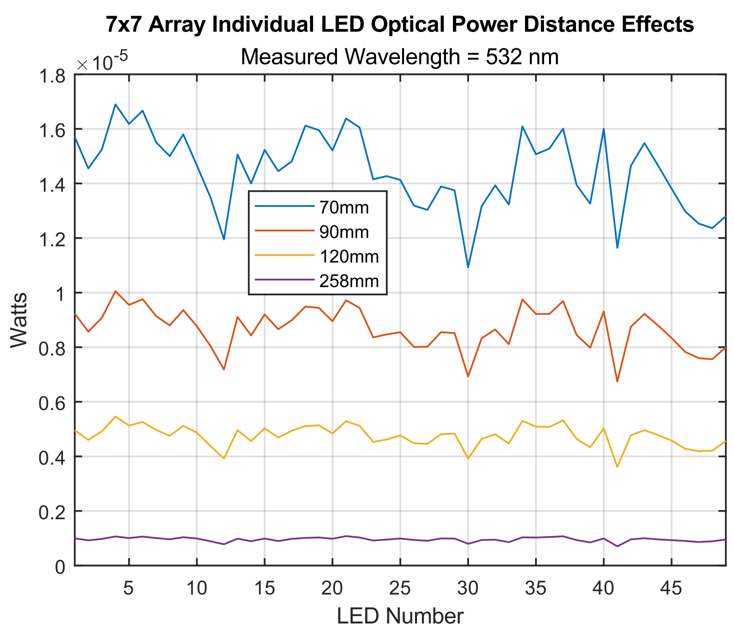

Figure 13: 7×7 grid optical power received by sample at various distances

Figure 11-12 shows the optical power received by the sample for each grid at the tested imaging distances. The optical sensor was placed where the sample slide would be, and the lights are illuminated in sequence without moving any components. The difficulty in this experiment is to make sure the sensor is directly above the center LED in the grid. To line up as close as possible, the calibration was completed as if to begin the capture phase to ensure centering on the grid, then the sensor was placed on the sample stage directly below the objective lens. This gives insight into which LEDs are having higher or outsized effects on the sample.

Note: when imaging the 7×7 matrix, the ribbon cable connector is placed on the PCB such that it contacts the sample stage plate before it can be placed right at 54 millimeters for consistency. As such, the 54-millimeter measurement was omitted for the 7×7 matrix.

4.2 EXPOSURE SETTINGS

In most images, it is desirable to set the exposure to a bright enough image that does not peak. However, since these images are taken at such a small scale, the light introduces a ripple effect as it passes around objects (Figure 14). As one of the ripples passes into the ripple bands from another source, they constructively interfere to create an additive brightness where they connect as in Figure 14 and Figure 15. The brightest point is around the edge of an object, and as the light moves around smaller objects, the brightest points are guaranteed to converge and risk peaking the brightness value (Figure 15). In order to counteract this effect, the exposure is dropped to allow this convergence to happen without (or limiting) maxing out the brightness at the pixel depth of 16-bits.

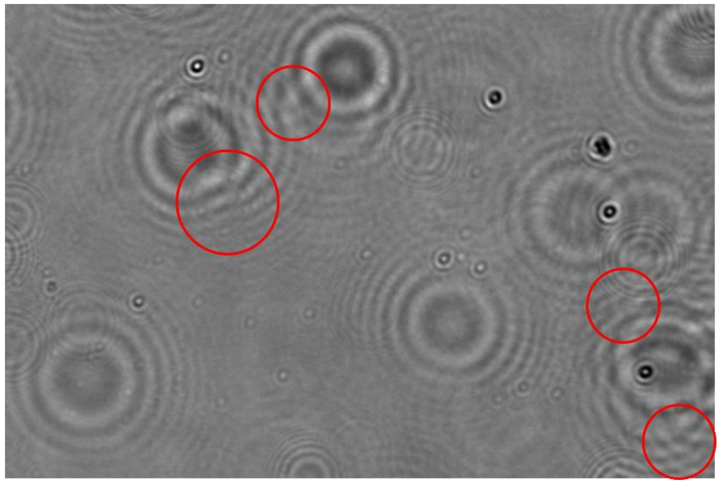

Figure 14: Constructive and destructive light waves on sample background

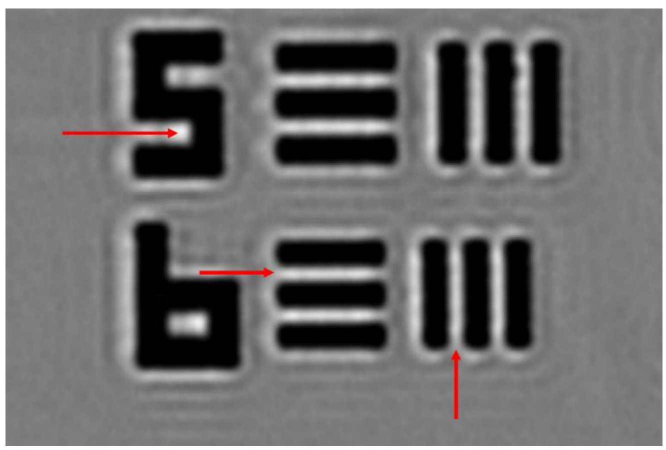

Figure 15: Constructive interference from sample image

As is made clear by Figure 11-12, there is a large difference between the sample-received illumination powers for each LED grid, so with each grid and their distance to the sample stage, a new exposure must be taken to avoid overexposing the image. Even if the majority of the pixel brightnesses are around 60% their maximum bit depth, they will have an outsized impact on peaking at the small scale our image is focused on (Figure 16).

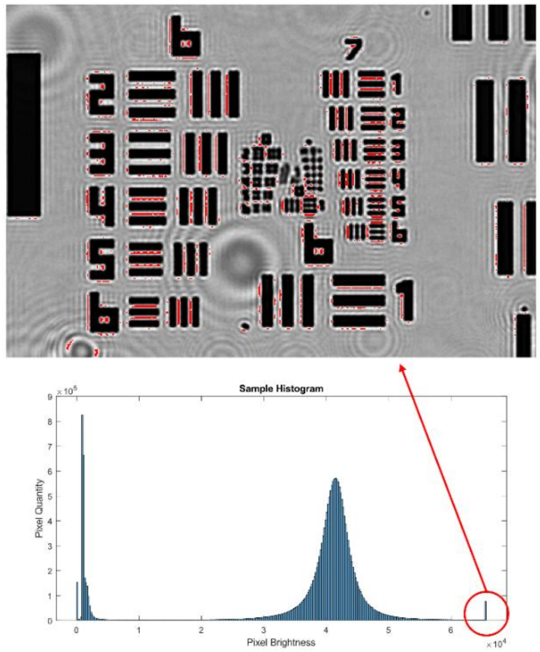

Figure 16: Histogram of sample with peak values highlighted in red

Using Mosaic’s built-in histogram viewer, while it does not provide an exact pixel count, it will show the histogram similar to Figure 16. While the center LED is on, the exposure setting is set so that the bulk of the pixels lies in the 30,000 range (out of the maximum 65,535). Ensuring that the histogram is closer to the middle values will give some confidence that the values are not going to peak before taking the picture.

It is worth mentioning that in Figure 9, the image capture settings in Mosaic are set to 49.93 milliseconds and with a gain set to 225. Without knowing the algorithm used for the gain adjustment, it is difficult to accurately determine the true values that were received by the sensor. Figure 9 was the center LED image taken which should have the highest concentration of photons on the sensor, and thus, a higher brightness. Taking that into account, for a visibly dim image, and a massive gain (225 out of a maximum of 257) the 32×32 grid relies heavily on both a lengthy exposure time as well as gain boost in order to produce visible images. While this achieves a reduction in exposure time, there is potential for some amount of distortion, and with the computational aspect of FPM acting on a pixel level, that distortion may propagate to false information shown in the final reconstruction.

Without knowing how the gain operates on the pixels, there cannot be a true comparison of the pixel brightness to LED brightness. As such, when the 32×32 grid is imaged, the gain is set to 1 so that the exposure time is the isolated variable of interest when comparing histograms. As a test of the 32×32 matrix, images were taken with a constant gain of 1. The height of the LED array changed, and the exposure time was roughly matched to create a similar histogram. Figure 17 shows the relationship of how the distance of the LED array will affect the exposure time on the 32×32 grid.

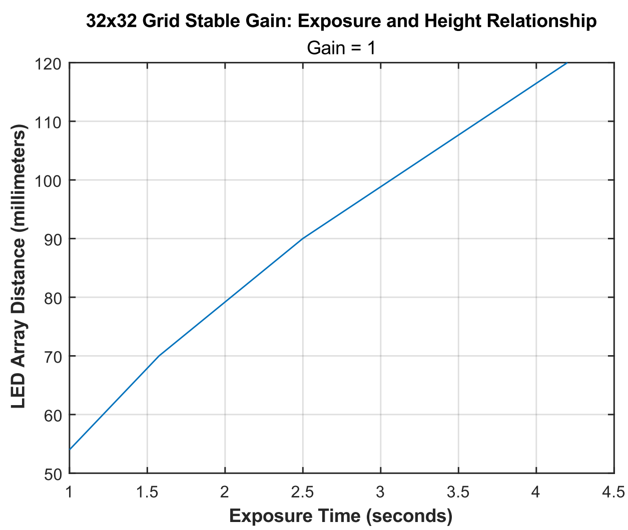

Figure 17: Array distance to exposure time relationship

Even with limited data, Figure 17 shows a resemblance to the inverse square law—where the further away the light source is, power received per unit area will fall off exponentially. Only in this case, rather than the incident power being measured, noting the exposure time required to attain a matching histogram profile. In other words, as the distance increases, the time required to expose the image increases. Figure 18 shows the same information, but for all three LED arrays. Take note of the flipped axes when compared to Figure 17.

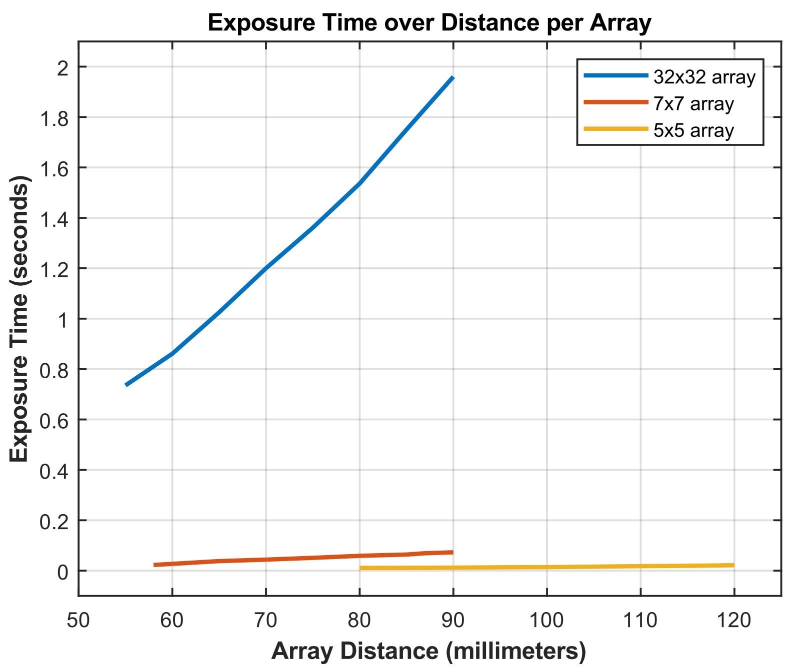

Figure 18: Required exposure time of center LED for each array at various distances

4.3 RECONSTRUCTION

To generate the reconstruction, the following parameters are input into the MATLAB FPM application: LED spacing, LED height, camera pixel size, wavelength, NA, and magnification. The combined magnification of the tube lens as well as the objective lens is 3, while the NA is fixed for the objective lens at 0.13. The camera's pixel size is 2.4 micrometers, and the green light wavelength is also fixed at about 530 nanometers, leaving the LED spacing and the LED height as the only variables that will change in the experiments.

The original 32×32 grid has a stable reconstruction using only the center 25 LED's shown in Figure 19.

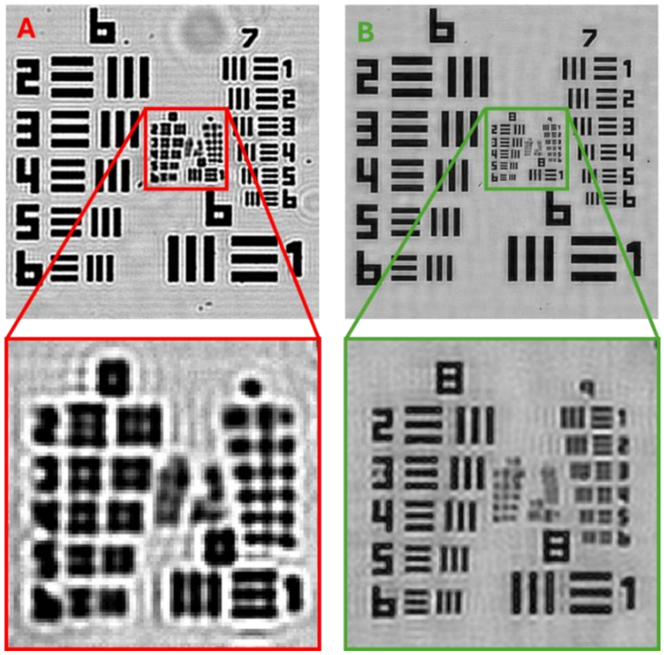

Figure 19: 32×32 Grid - 25 LED Reconstruction: A) Center LED Image. B) Reconstructed Image

The image capture settings for Figure 19 reflect a 199.358 millisecond exposure time at a 54-millimeter distance from the sample. In Part A of the figure, the desynchronization is visible in the image before FPM reconstruction, while much smaller and less apparent than in Figure 9, it still shows a constant horizontal banding pattern. In Part B, the reconstructed image has seemingly removed the desynchronization lines. Referring to the manufacturers data sheet for the sample slide (Table 2), in the center LED image, the smallest distinguishable feature is in the range of Group 7 Element 6 to Group 8 Element 1 (1.953 microns), while the reconstruction resolves features around Group 9 Element 1-2 (0.870 microns).

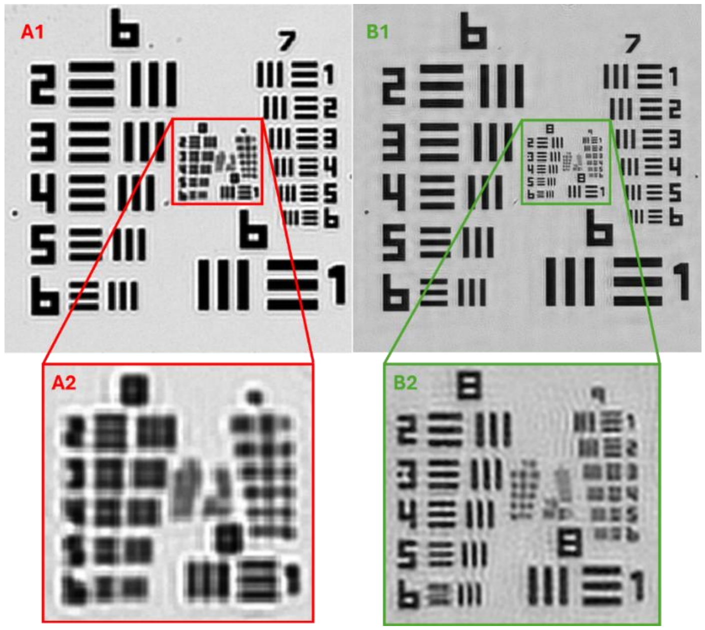

Figure 20: Custom 5×5 Matrix Reconstruction. (A1) Center LED Input Image of Group 6 & 7. (A2) Center LED Input Image of Group 8 & 9. (B1) FPM Reconstruction of A1. (B2) FPM Reconstruction of A2

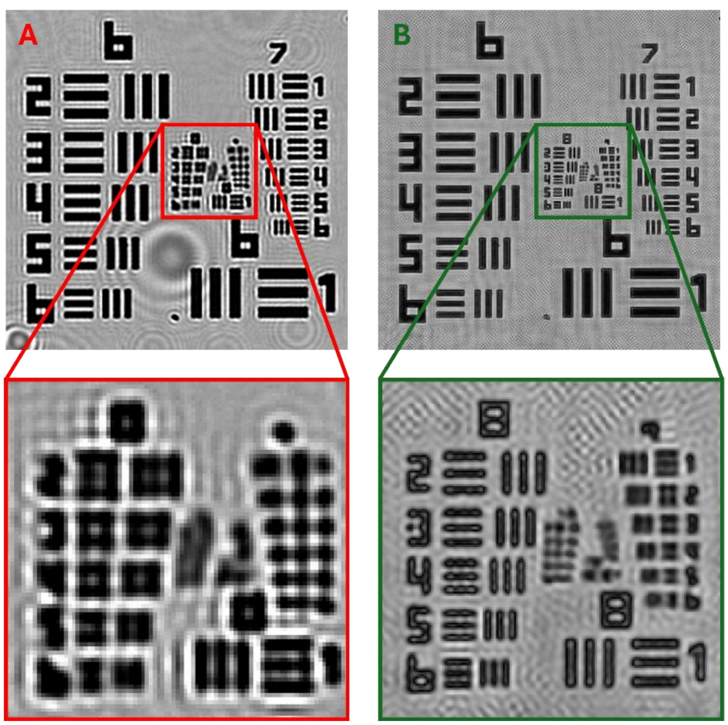

Figure 21: 7×7 Grid - 25 LED Reconstruction. (A) Center LED Image. (B) Reconstructed Image

For Figure 20 and Figure 21, the custom matrices show a similar quality final image, but with the caveat of having a preferred distance from the sample stage. In order to get the best quality reconstruction there needs to be an appropriate array size and distance to cover enough bright and dark field. If only the bright field is taken, the result will look like Figure 22 (B). However, adding an additional perimeter of lights (i.e., going from 5×5 to 7×7) there is an increase in the resolution Figure 22 (C). The following figure shows the same data set, but with (B) trimmed to only the center 25.

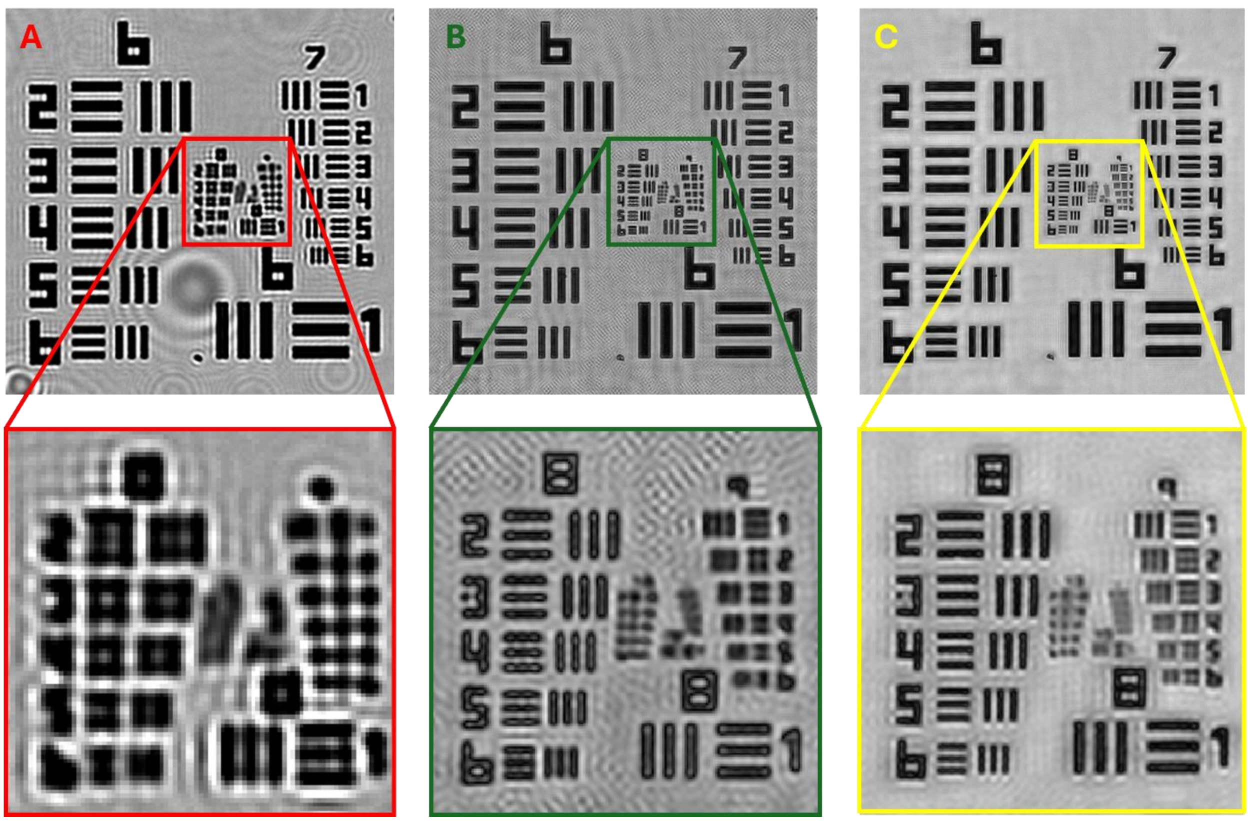

Figure 22: 7×7 Grid Reconstruction of different grid sizes. (A) Center LED Image. (B) 25 LED. (C) 49 LED

The following figures are of each grid in order of closest to furthest distance from the sample stage:

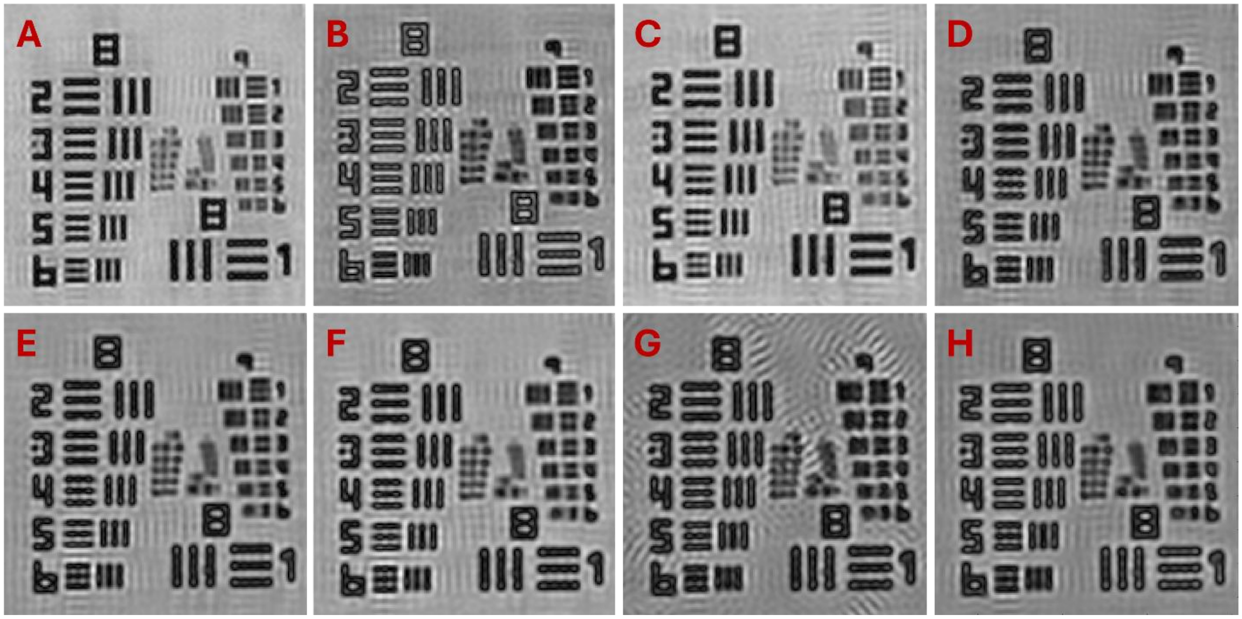

Figure 23: 32×32 Grid Reconstructions at heights A) 55mm B) 60mm C) 65mm D) 70mm E) 75mm F) 80mm G) 85mm H) 90mm

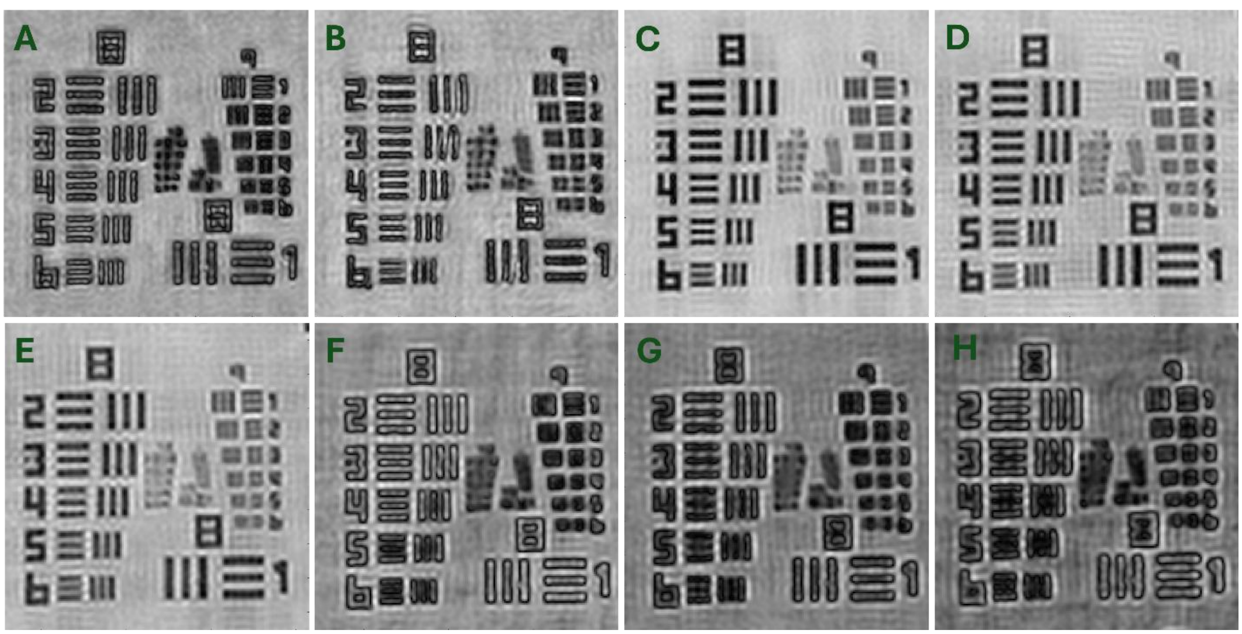

Figure 24: 5×5 Grid Reconstructions at heights A) 80mm B) 90mm C) 95mm D) 100mm E) 105mm F)110mm G) 115mm H) 120mm

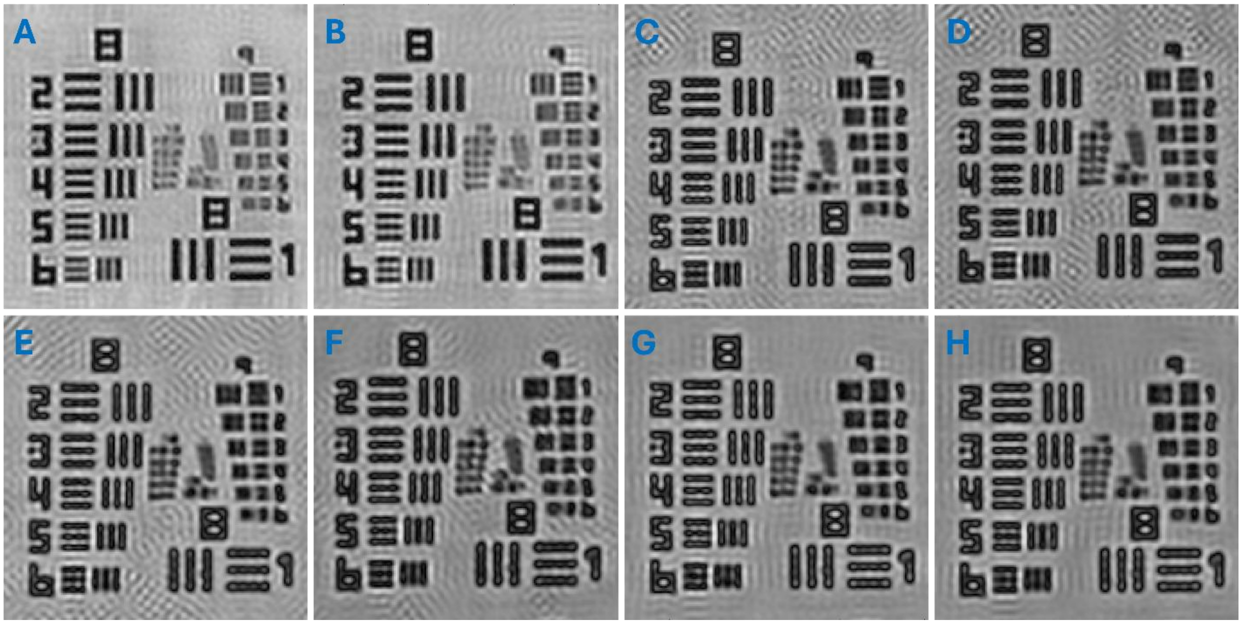

Figure 25: 7×7 Grid Reconstructions at heights A) 58mm B) 65mm C) 70mm D) 75mm E) 80mm F) 85mm G) 87mm H) 90mm

Among each of the grids using 25 LEDs to generate a reconstructed image, they each produced a similar minimum size to about Group 9 Element 2, about 0.870 microns. Depending on the distance and inter-LED spacing, the quality of the reconstruction varies, with a notable exception of the 5×5 array producing some artifacts inconsistent with the other arrays. The next chapter will look into the finer details of the results as well as indicate the larger systemic issues with each arrangement of LEDs.

CHAPTER 5: DISCUSSION

5.1 PCB DESIGN

When designing the LED arrays, one of the major design considerations was the production and assembly convenience. In this experiment, there were few of the conveniences that are present in commercial PCB manufacturing processes, such as minimum trace sizes, protective coatings, and vias. For any given array size used, whether it be a 5×5 or potentially a 13x13 or larger, adding more LEDs has the added benefit of being able to produce a greater reconstruction quality, despite the density of the grid, which may not be as critical as initially thought.

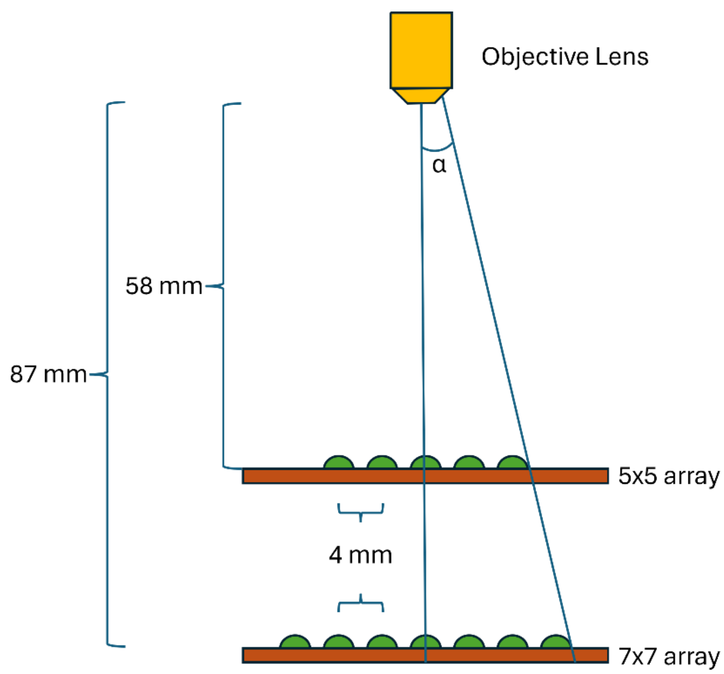

Figure 26: Illustration of similar array geometry

Figure 26 illustrates the similar geometries that can be used to determine a change in quality based on grid density. Both arrays have the same LED spacing, but at an increased distance, one extra LED spacing around the perimeter of the grid gives the same field of view to the extent of the array but now has a higher density of LEDs per. Nearly doubling the LEDs has no recognizable effect on the outcome as seen in Figure 27.

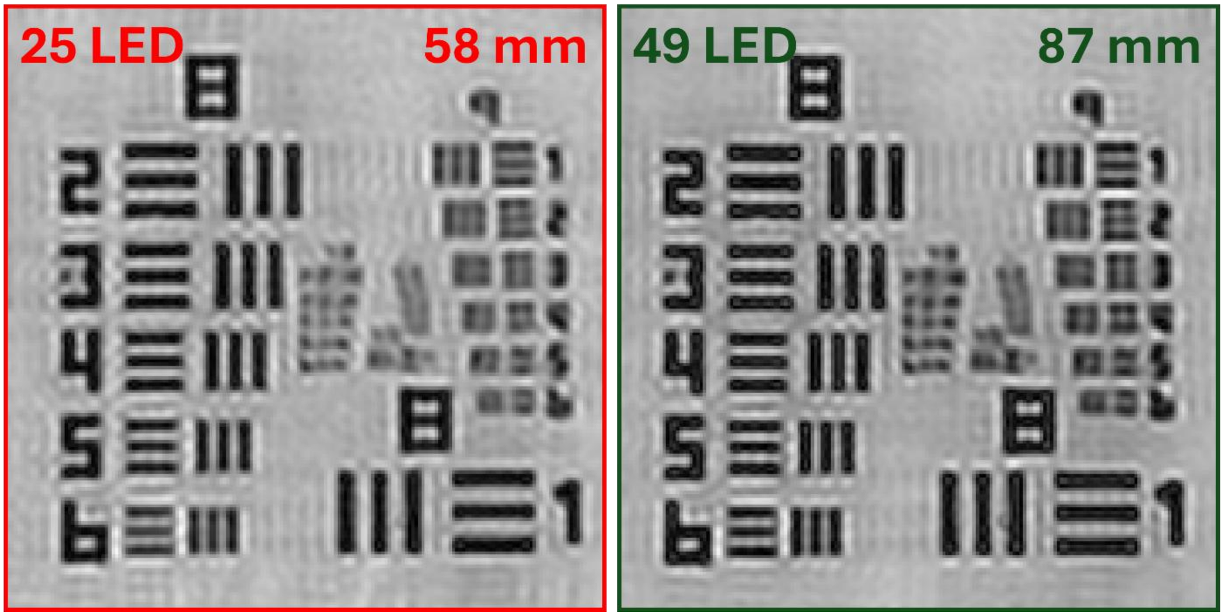

Figure 27: Grid density comparison (LEFT) 25 LEDs at 58mm (RIGHT) 49 LEDs at 87mm

In future iterations of a custom PCB grid, this would be considered to find a suitable middle ground between density and quantity for the type of LED used.

5.2 LED TYPE

In the experiment, three types of LEDs were used: RGB surface mount on the 32×32 grid, 0608 surface mount on the 7×7 grid, and a 5-millimeter bulb through-hole on the 5×5 grid. Each LED had a unique optical power as shown in several ways throughout this thesis. In the direct-contact measurement of the optical power, the 0608 LEDs emitted more power than the bulb type.

As the distance increased, however, the bulb type sustained its power output. This is because the surface mount type used in the experiment has a broader illumination angle, where its power is spread out over a larger area. The bulb type is made in such a way that it reflects light more narrowly in the direction orthogonal to its base, carrying most of its energy in that direction (Figure 28).

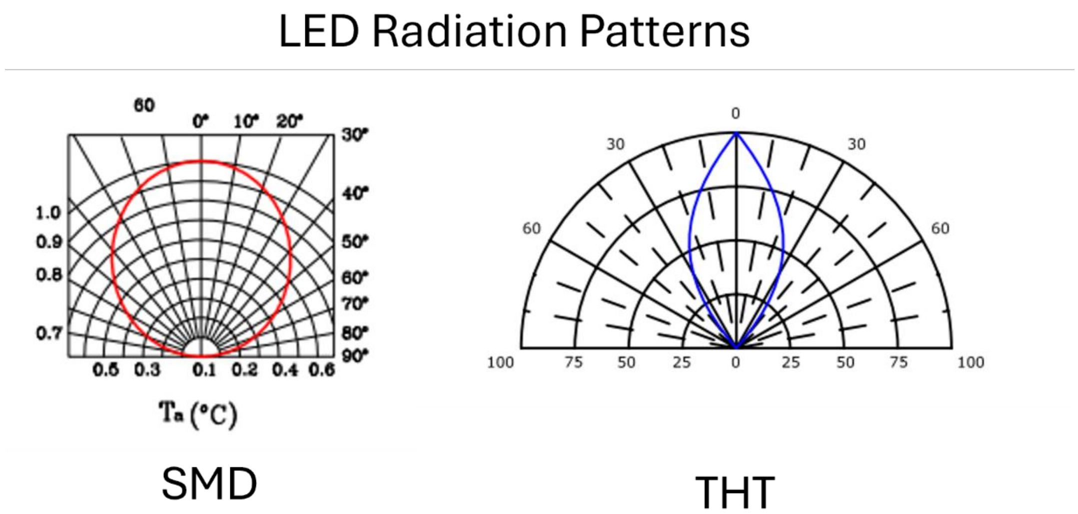

Figure 28: (LEFT) Surface mount (RIGHT) Through-hole bulb-type LED radiation patterns

5.3 OPTICAL POWER OUTPUT

In addition to the LED type, there are two other contributors to how bright the LED was. Firstly, the resistors used in series with the LEDs in this experiment were allowed to run high, 10-20 milli-Amps on direct current, which is the safe current rating of the LEDs as well as for one I/O pin on the Arduino board. Maximizing within the datasheet specifications produces the greatest brightness, and thus a greater reduction in the exposure time per image.

The other contributing factor that changed in the updated boards was moving away from PWM to operate on direct current. Going from 5% duty cycle to 100% duty cycle was, no doubt, a massive boon to the reduction in exposure time. However, given the drastic results of the exposure time as reported by this thesis, there can be some common ground of allowing a larger grid that uses multiplexing to some degree. Given that only one LED is on at a time (in this method of FPM) and based on previous multiplexing research [2, 3] it would be reasonable to assume no more than 5 LEDs would be on at any one time. Without the additional strain of potentially operating 1024 LEDs simultaneously, as is the case with the 32×32 array, the duty cycle for a future board could conceivably be much higher at around 20-50% based on the multiplexing method.

In the power output received by the 5×5 array, there was a notable drop in power, annotated in Figure 29.

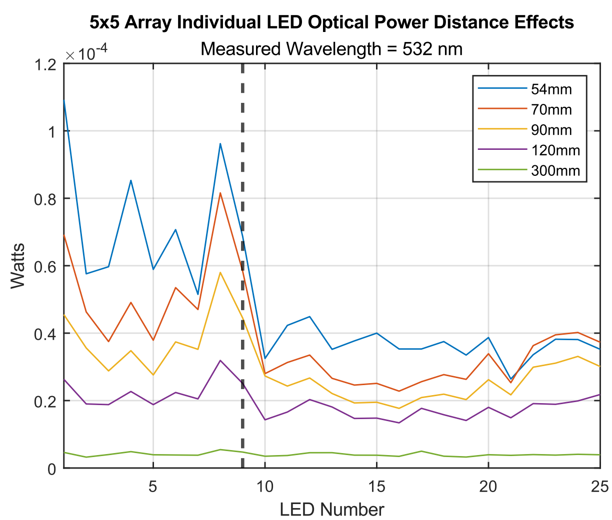

Figure 29: 5×5 Array optical power output annotated with drop-off

The closer the array was to the sample stage, the more dramatic the fall-off of power output was registered. Note that the highest values occur on LEDs 1-9. These LEDs make up the center 3x3 spiral when illuminating in sequence, and therefore have their beam centers pointed directly, or nearly directly onto the sample. The following LEDs outside of the center 3x3, are pointing up and near the sample, thus only the side of the main lobe of power is captured, reducing the power received by nearly half in some cases. The exaggerated amplitude of the very-bright LEDs in combination with being close to the sample stage can also be visualized with the illustration in Figure 6.

One issue with the 5×5 array is indicated by the large spike in brightness on LED 8. Either due to a slight tilt of the LED as it was soldered onto the board, or just a natural variation of LED quality. In general, the bulb LEDs had the highest change of power output from one LED to the next. LED 8 being much brighter than LED 1 could have been the largest contributing factor in the reconstruction artifacts seen. This effect is also noted in [11].

The difference in the magnitude of power per array are in Figure 30. When accumulating the data, the 32×32 board was tested at a near distance of 54 millimeters, and a point far outside of the reasonable range at 120 millimeters which would require an exposure time of over 4 seconds based on the established testing parameters. The 7×7 array was first tested at its most optimal range, then was tested to see at what distance it matched the 32×32 array maximum at 54 millimeters. The 7×7 array would need to be placed over 4.5x the distance of the original to get the same power reading at the closest marker for the original grid (Figure 30).

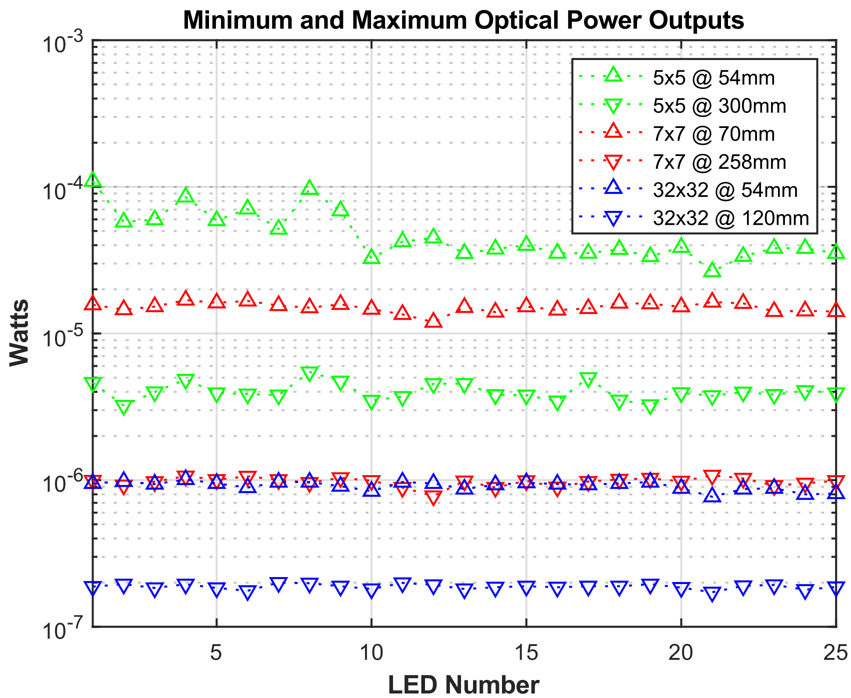

Figure 30: Minimum and Maximum Optical Power Values for each LED matrix

When the 5×5 grid was tested under the same circumstances, the microscope set up maximized its distance from the grid to sample at around 300 millimeters and still yielded a power greater than the maximum output of the 32×32 grid.

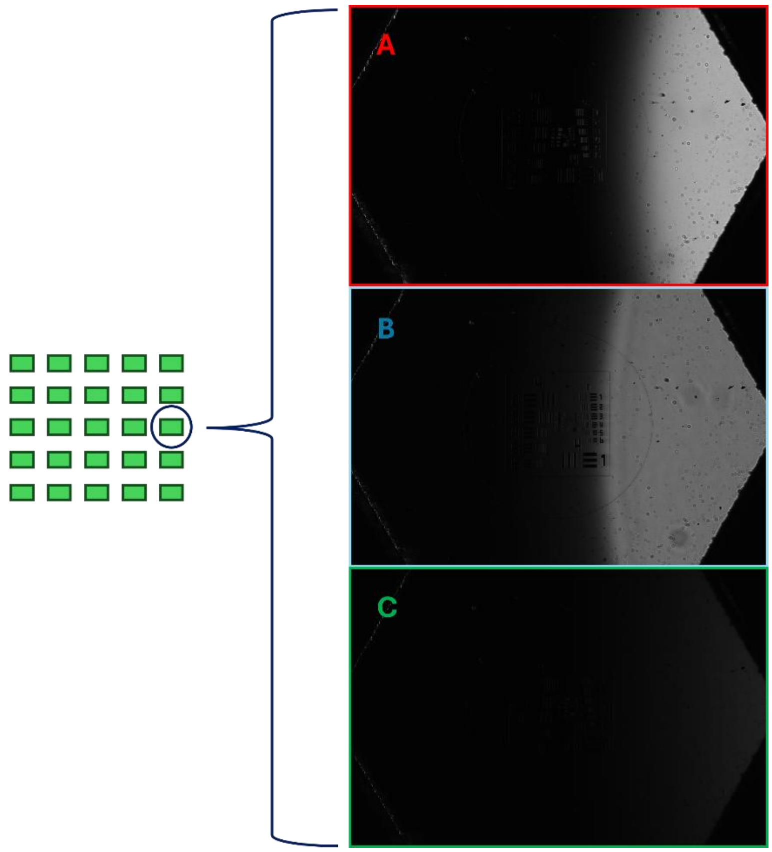

Figure 31: 11th LED Illumination from raw image (A) 32×32 grid (B) 7×7 grid (C) 5×5 grid

Figure 31 illustrates the differences in the sharpness of the dark field. Each part of the figure has the 11th LED illuminated which is positioned in the same location in the dark field for each board's respective geometry. (A) has a soft edge potentially due to the larger surface area of the LED face. (B) has the sharpest edge to the dark field transition, most likely associated with the small light source. (C) is at the opposite extreme with an exaggerated gradient from bright field to dark field. The large size of the LED bulb along with its effective 'glowing' through subsurface scattering on the nearby bulbs likely causes this gradient effect.

5.4 EXPOSURE TIME REDUCTION

As shown in Figure 18, there is a dramatic decrease in exposure time when comparing the custom arrays to the original off-the-shelf array. As previously stated, the $R_{overlap}$ plays an important role in the quality of the reconstruction, as does the maximum illumination angle. To ensure a fair comparison of exposure time reduction, the comparison will only account for a 25 LED data sample (the 5×5 array maximum), and the maximum illumination angle must match so that there is equivalent coverage of the bright and dark fields.

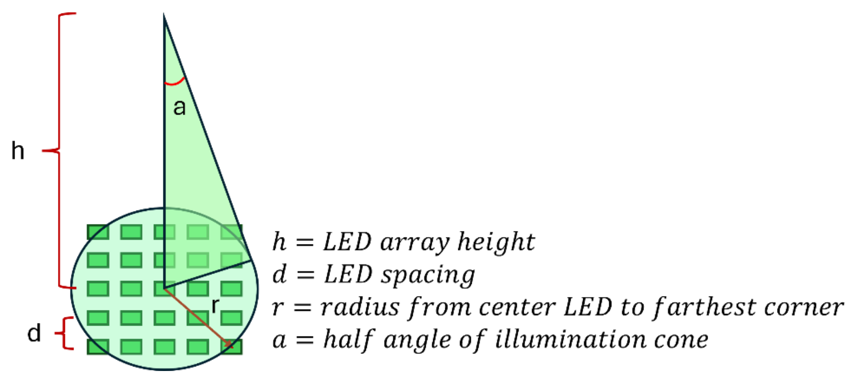

Figure 32: Illustration of illumination variables

Using Figure 32 as reference, we can determine the variables using obtained data from the 32×32 grid, making sure to choose a height that bodes well for reconstruction. Setting $d = 4\,mm$ and $h = 55\,mm$, the radius from the center LED to one of the outer corner LEDs is r = $\sqrt{(8mm^2 + 8mm^2)} = 11.31$ mm. The half angle $a = arcsin\left(\frac{11.31mm}{\sqrt{11.31mm^2+55mm^2}}\right) = 11.62°$. The same parameters can be used by the 7×7 array as it shares the same geometry as the 32×32 grid. However, for the 5×5 grid we use can deduce the required height to match the same half angle a. The equivalent height for the 5×5 grid would be $h = 96.28\,mm$. However, our closest matching data set is 95 millimeters. So, for our comparison of exposure times, the image sets acquired at the closest point to the calculated heights will be chosen.

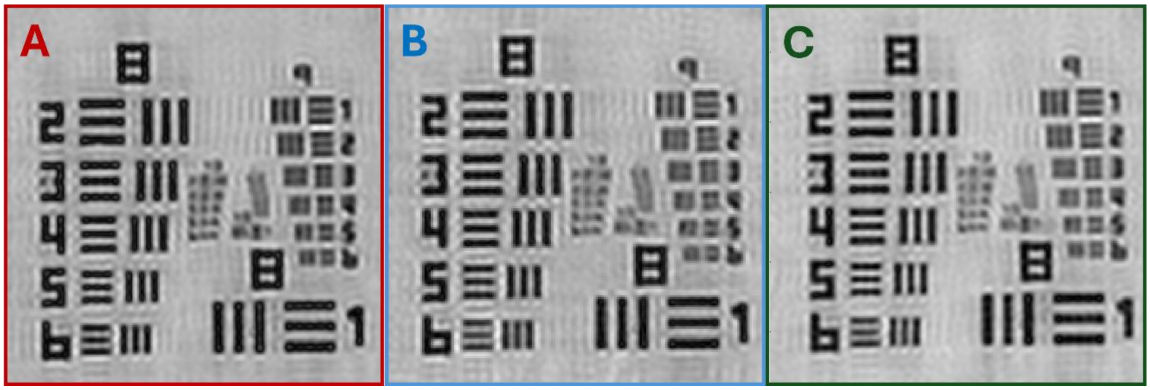

Figure 33: (A) 32×32 grid at 54 mm (B) 7×7 grid at 58 mm (C) 5×5 grid at 95 mm

Figure 33 shows the data sets closest to the calculated values. Each of them has a very similar quality, however they vary drastically in exposure time (Table 3).

LED Array	**Exposure Time (seconds)**
32×32	0.735055
7×7	0.022669
5×5	0.013335

Table 3: Exposure time comparison across all boards

Extrapolating from the exposure data for similar results, with the original 32×32 grid being the baseline, there was a 92.02% reduction in exposure time with the surface mount LED (7×7 grid) and 98.19% reduction in exposure time (5×5 grid) per image.

CHAPTER 6: CONCLUSION

Changing the variables of the LED arrays for FPM has a large impact, not only on the final reconstruction of the images, but also within the image collection phase itself. Notable mentions of changes are the LED geometry and the importance of keeping similar ratios of inter-LED spacing and array height. Having more LEDs and a denser grid space does not necessarily increase the quality of the final image and could result in wasting the time saved by other upgrades. For example, going from a 25 LED capture phase to a 49 LED capture phase may not provide tangible benefits as in Figure 27.

6.1 ANSWERS TO RESEARCH QUESTIONS

The most impactful changes made from the original 32×32 grid is changing to direct current instead of 5% duty cycle of PWM. The easy access to the grid as well as the Arduino UNO R3 makes it a great fit for FPM—especially for use cases that require large grid sizes. The drawback is that it was designed to have up to 1024 LEDs on at a given time. As such, safety measures were incorporated in the design of the board to prevent a user from over-drawing current. For the very small number of LEDs used in FPM, a more liberal allowance of current draw or duty cycle is more appropriate.

Allowing LEDs to draw more current and give off more light output is the other contributor to reducing the exposure time. A corollary to the additional total power is being able to direct the optical power in a directed fashion as is inherent in the bulb-type LEDs. This provides incredible range in the limited use cases for when that may be needed. For a reasonable distance of between 50 and 100 millimeters, reducing the exposure time from 92-98% adds to the FPM field and can be used by future researchers to take the findings from this thesis to the next level.

6.2 FUTURE WORK & RECOMMENDATIONS

As stated, there are many potential improvements to the FPM field. Exposure time is only one of the issues that contributes to the time bottleneck. Based on the experimentation and discovery of this thesis, incorporating the new design features with the promising results of multiplexing can compound the timing reduction to an even greater reduction.

In the hardware, my recommendation is to design with the surface mount LEDs in mind. Using a relatively high but safe current rated on the LED and microcontroller will allow for the best reduction in exposure time. If designing for a large grid where the sum of row and columns is greater than the available I/O on the microcontroller, testing PWM multiplexing with high duty cycles (20-50%), or an addressable LED array could yield good results while vastly expanding the FoV of the array and grid density.

Any future designs using bulb-type LEDs should incorporate a shielding mechanism that blocks the light bleeding and causing a subsurface scattering glow on nearby LEDs or should be physically spaced out enough to avoid that issue. Additionally, experimenting with methods of guiding the main radiation pattern of the bulb to shine on the sample may yield more powerful results. Keeping the LEDs raised off the board with a slight bend in the direction of the center or using a non-planar board design through 3D printing a scaffold and wiring connections manually.

The software used in this experiment was simple and relied on manual inputs through a serial terminal. To automate and better calculate total capture times, designing a piece of control software to manage image capturing as well as changing the LED to the next in sequence would be of great benefit.

REFERENCES

[1] G. Zheng, R. Horstmeyer and C. Yang, "Wide-field, high-resolution ptychographic microscopy," *Nature Photonics,* vol. 7, pp. 739-745, 2013.

[2] L. Tian, X. Li, K. Ramchandran and L. Waller, "Multiplexed coded illumination for Fourier Ptychography with an LED array microscope," *Biomedical Optics Express,* vol. 5, no. 7, pp. 2376-2389, 2014.

[3] B. Lin, J. Zhao, G. Cui, P. Zhang and X. Wu, "Efficient multiplexed illumination and imaging approach for Fourier ptychographic microscopy," *Journal of the Optical Society of America A,* vol. 39, no. 5, pp. 883-896, 2022.

[4] J. Sun, C. Zuo, L. Zhang and Q. Chen, "Resolution-enhanced Fourier ptychographic microscopy based on high-numerical-aperture illuminations," *Scientific Reports,* vol. 7, p. 1187, 26 April 2017.

[5] M. G. Mayani, N. Hussain, D. W. Breiby and M. N. Akram, "Improved resolution Fourier ptychography schemeusing oil-filled dome-shaped LED array," *Electronics Letters,* vol. 58, no. 20, pp. 762-764, September 2022.

[6] J. Sun, Q. Chen, Y. Zhang and C. Zuo, "Sampling criteria for Fourier ptychographic microscopy in object space and frequency space," *Optics Express,* vol. 24, no. 14, pp. 15765-15781, 2016.

[7] S. Dong, Z. Bian, R. Shiradkar and G. Zheng, "Sparsely sampled Fourier ptychography," *Optics Express,* vol. 22, no. 5, pp. 5455-5464, 2014.

[8] Y. LeCun, Y. Bengio and G. Hinton, "Deep Learning," *Nature,* no. 521, pp. 436-444, 2015.

[9] T. Nguyen, Y. Xue, Y. Li, L. Tian and G. Nehmetallah, "Deep learning approach for Fourier ptychography microscopy," *Optics Express,* vol. 26, no. 20, pp. 26470-26484, 2018.

[10] S. Jiang, P. Song, T. Wang, L. Yang, R. Wang, C. Guo, B. Feng, A. Maiden and Z. Guoan, "Spatial- and Fourier-domain ptychography for high-throughput bio-imaging," *Nature Protocols,* vol. 18, no. 7, pp. 2051-2083, 2023.

[11] Z. Bian, S. Dong and G. Zheng, "Adaptive system correction for robust Fourier ptychographic imaging," *Optics Express,* vol. 21, no. 26, pp. 32400-32410, 2013.

APPENDICES

Figure 34: Google Maps estimated distance of focal target

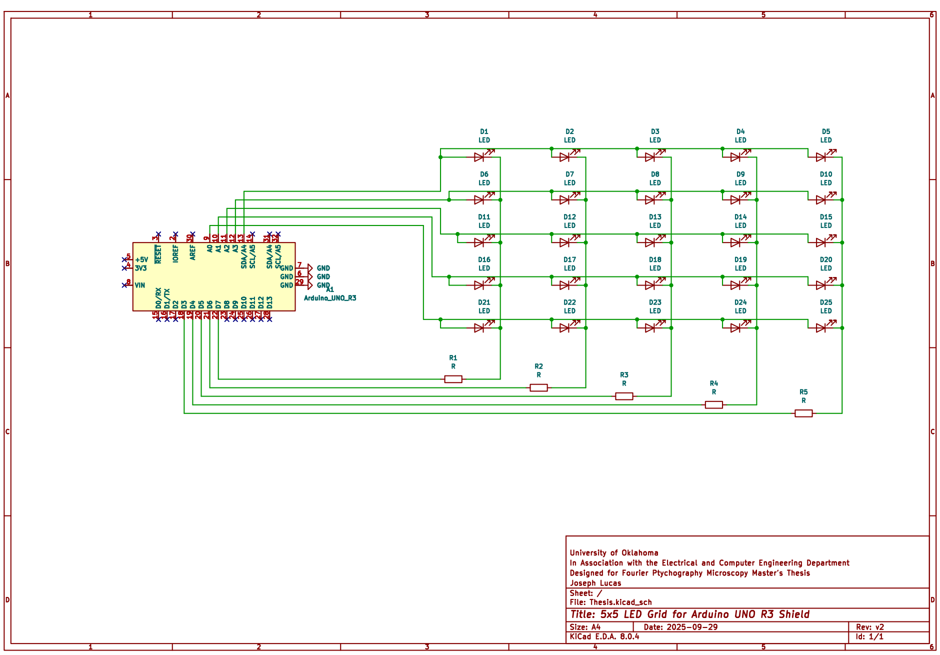

Figure 35: 5×5 LED Matrix Schematic

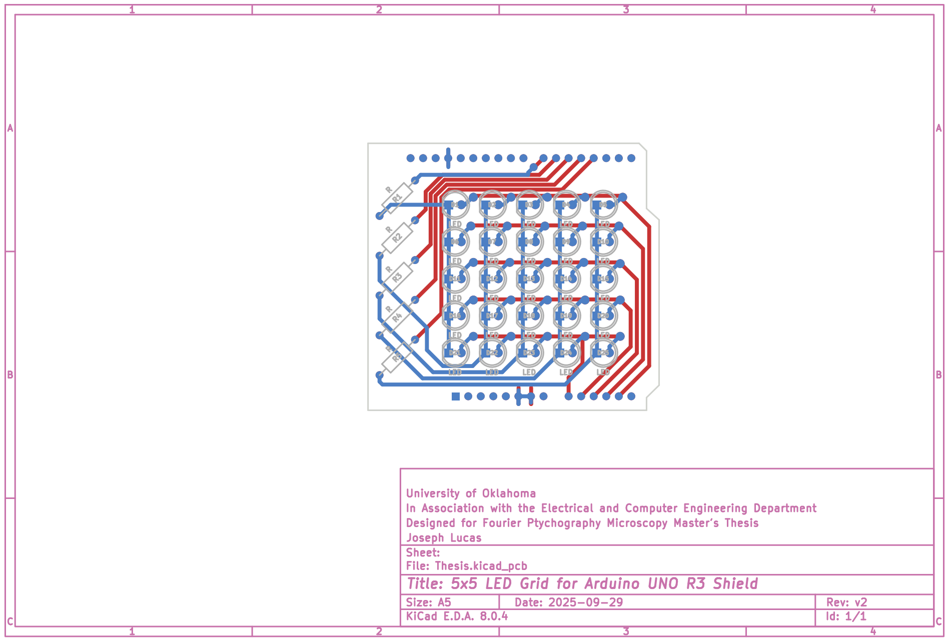

Figure 36: 5×5 LED Matrix PCB

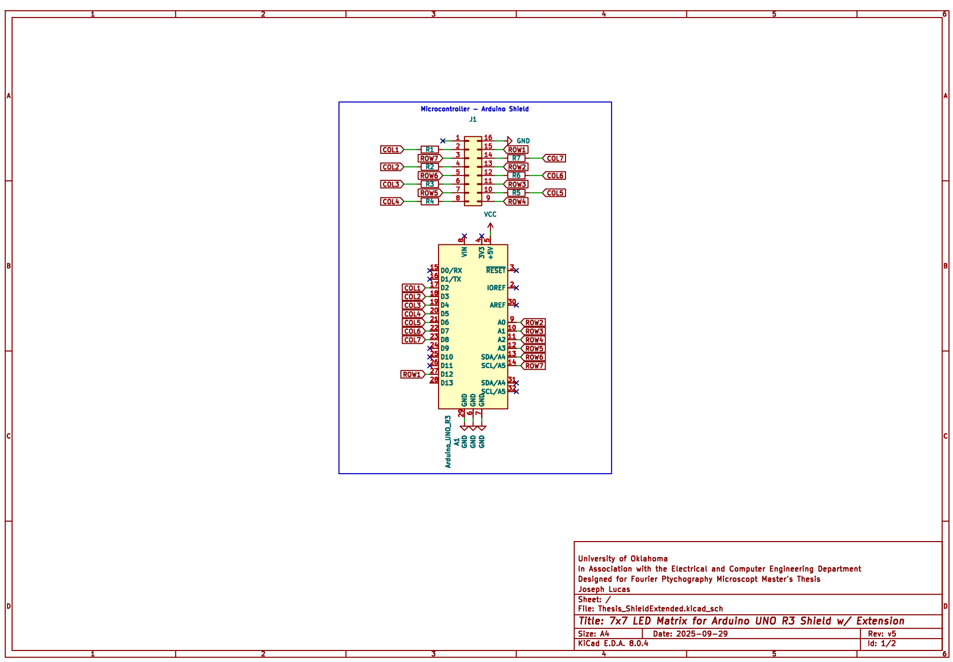

Figure 37: 7×7 LED Matrix Schematic – Arduino Shield

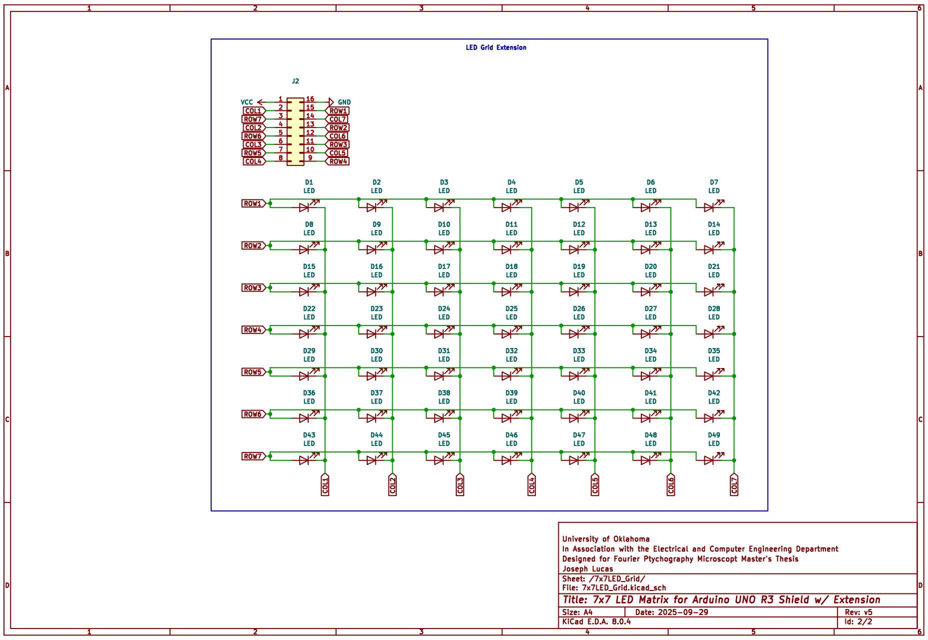

Figure 38: 7×7 LED Matrix Schematic - Shield Extension

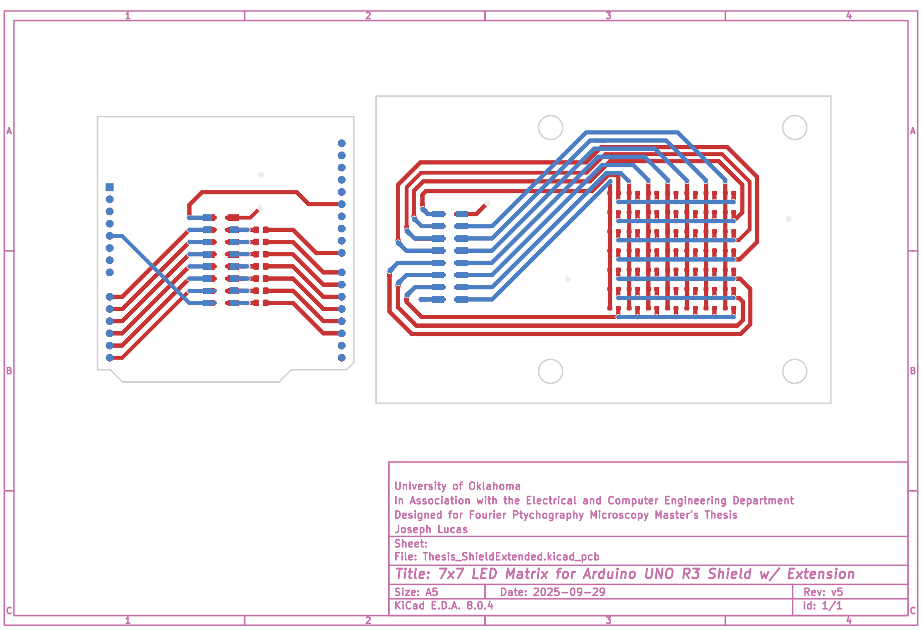

Figure 39: 7×7 LED Matrix Circuit Schematic